RESEARCH PAPER

Analysis of heat transmission in convective, radiative and moving rod with thermal conductivity using meta-heuristic-driven soft computing technique

Naveed Ahmad Khan[1] · Muhammad Sulaiman[1] · Fahad Sameer Alshammari[2]

Abstract

The present study analyzes the thermal attribute of conductive, convective, and radiative moving fin with thermal conductivity and constant velocity. The basic Darcy's model is utilized to formulate the governing equation for the problem, which is further nondimensionalized using certain variables. Moreover, an effective soft computing paradigm based on the approximating ability of the feedforword artificial neural networks (FANN's) and meta-heuristic approach of global and local search optimization techniques is developed to quantify the effect of variations in significant parameters such as ambient temperature, radiation-conduction number, Peclet number, nonconstant thermal conductivity, and initial temperature parameter on the temperature gradient of the rod. The results by the proposed FANN-AOA-SQP algorithm are compared with radial basis function approximation, Runge–Kutta–Fehlberg method and machine-learning algorithms. An extensive graphical and statistical analysis based on solution curves and errors such as absolute errors, mean square error, standard deviations in Nash–Sutcliffe efficiency, mean absolute deviations, and Theil's inequality coefficient are performed to show the accuracy, ease of implementation, and robustness of the design scheme.

Graphical Abstract
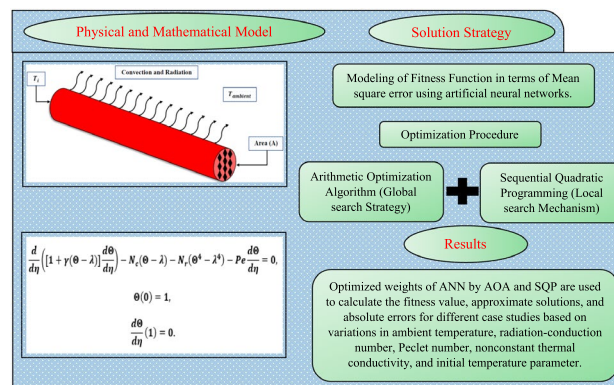
Keywords Heat transfer · Moving porous fin · Moving rod · Metaheuristics · Deep learning · Artificial intelligence

✉ Muhammad Sulaiman
msulaiman@awkum.edu.pk

Extended author information available on the last page of the article

1 Introduction

Heat transmission is the phenomenon used to explain heat transfer from higher temperatures toward lower concentrations (Gireesha and Sowmya 2020). In recent years, the process of heat transfer has emerged as the most important subject in the field of thermal engineering due to the prediction

of heat exchanger in variety of circumstances including solar collector, gas turbines, radiators in cars, and energy production (Alkam and Al-Nimr 1999; Deshamukhya et al. 2018; Sowmya et al. 2019; Khan et al. 2021d). The heat exchangers or extended surfaces are an integral part of any device that generates heat during its working process. They are used to increase the heat transfer rate from surfaces cooled by gases under natural or forced convection. Usually, heat transfer occurs through the mechanisms of conduction, convection, and radiation, or a combination of these methods (Ma et al. 2017; Sun and Li 2020). Many studies on extended surfaces have been conducted, and some examples are provided in the references (Ye 2017; Ben-Nakhi and Chamkha 2006; Khan et al. 2021c; Chamkha et al. 2010). To improve the rate of heat transfer, the fins are designed using a porous medium such as sintered powder or perforated plates and metal sponge so that it can be easily used in critical systems. The porous heat exchangers are commonly used in powerful lasers, spacecraft thermal management systems, phased-array radar systems, industrial furnaces, and catalytic-chemical particle beds.

During the course of the last decade, the analysis of fins with the purpose of enhancing heat transmission has attracted the interest of a great number of researchers. When the cross-sectional area of a fin is not very large, there is not a significant difference in temperature throughout the cross-section. Then the only direction in which it undergoes a significant change in temperature is the one that corresponds to the length of the fin. To put it another way, the temperature field over the length of the fin is a one-dimensional field, despite the fact that it fluctuates in temperature as it travels down the length of the fin. A number of researchers have made various contributions toward the development and the enhancement in heat transmission of a one-dimensional porous structure with thermal conductance. An earlier study was conducted by Hung and Appl (1967) to investigate how heat is transferred within straight fins with internal heat generation. Razelos and Kakatsios (2000) studied the radiation effects of rectangular fins, which is quite significant in the design of reliable equipment, gas turbines, and nuclear plants. Further, the concept of heat transmission through porous fins was presented by Kiwan and Al-Nimr (2001), which was later improved by using Darcy's model to formulate the mathematical models of heat transfer in porous mediums (Kiwan 2007; Kiwan and Zeitoun 2008). Heat transfer through a porous fin in a nanofluid subjected to convective and radiative environments was examined by Baslem et al. (2020). They examined the effect that heat transport via convection and radiation had on the fin. They concluded that the heat transmission from the fin is greatly improved with the use of the Cu-water nanofluid compared to Al_2O_3-water and TiO_2-water nanofluids. Taklifi et al. (2010) studied the influence of magnetohydrodynamics

(MHD) on heat transfer in rectangular fin. Their analysis indicates that the heat transfer rate decreases by employing the effect of MHD near the tip of the fin. Selimefendigil and Öztop (2012) predicted heat transport through a square cavity in the presence of an adiabatic thin fin using a fuzzy-based model.

In airborne and space applications, trapezoidal, triangular, and concave parabolic features, which result in a lighter design, are preferred than rectangular fins of equivalent size. This is because these characteristics result in a more efficient distribution of the heat over the fin. On the other hand, fin structures with a thinner profile are more difficult and costly to manufacture (Buonomo et al. 2021; Kiwan et al. 2020). In last few decades, several researchers have worked in this area by considering different fin profiles to improve the heat distribution performance of the fins. Aziz and Makinde (2010) examined the entropy generation and thermal performance of two-dimensional orthotropic pin fins used in advanced light weight heat sinks. The Darcy model and the LTE assumption were utilised for the research that was conducted by Ndlovu and Moitsheki (2018) on a porous pin fin that was subjected to natural convection heat transfer. The research conducted by Turkyilmazoglu (2018) focused on heat transmission from moving exponential fins that have internal heat production. The exact formulae for the thermal aspects, such as the distribution of temperature, as well as the efficiency, were developed and studied. Fox et al. (1969) was among the first to do an analytical study on the heat transmission of moving fins in a non-Newtonian fluid. The rigorous impact of the Cattaneo-Christov heat flow model on thermal conductivity, internal resistance and magnetic stagnation of non-Newtonian fluids,has been studied by Zhao et al. (2021).

Most of the physical phenomena that emerge in the real world, especially the occurrence of heat and mass transfer under diverse effects, are well recognized and modeled as nonlinear differential equations (Das and Kundu 2020). In this regard, various numerical and analytical techniques are developed to study the temperature distribution. The homotopy perturbation method was adopted by Domairry and Fazeli (2009); Cuce and Cuce (2015); Hoshyar et al. (2015) to detect the fin efficiency of variable thermal conductive longitudinal fin. In order to get the solutions to the heat equation describing a rectangular contoured circumferential fin, Sarwe and Kulkarni (2021) used the idea of the differential transformation approach. The effect of environmental temperatures such as convective sink temperature, radiative sink temperature, as well as the impact of the heat production number on the distribution and temperature profile of a convective-radiative stationary fin was studied by Pranab KantiRoy using Adomain decomposition method (ADM). Tejani et al. (2017, 2019a) proposed an approach called the modified

heat transfer search (MHTS). This method combines sub-population-based simultaneous heat transfer modes such conduction, convection, and radiation. This was done in order to investigate the dynamic behaviour of the structures and remove vibrations that had not been meant to be there. Patel and Meher (2015) have revisted the traditional Adomian decomposition method and modified the technique by including the adjustment parameters for controlling the convergence of solutions to highly nonlinear porous structures with different profiles of conductance. Similarly, the M. Matinfar, solved the nonlinear unsteady mathematical model of the convective-radiative equation and a nonlinear convective-radiative-conductive equation by adjusting the small parameters ϵ_1 and ϵ_2 with modified variational iteration method and He's polynomials. The homotopy analysis method was applied by Moitsheki et al. (2015); Dinarvand and Hosseini (2013) for predicting the changes in thermal behaviour of the porous fin with thermal conductance. The impact of thermal conductivity with magnetic field on straight rectangular fin with insulated tip and nanofluid was studied by using the Akbari-Ganji's method (AGM) (Hosseinzadeh et al. 2022). Sobamowo et al. (2019) implemented the finite difference method (FDM) to examine the impact of compositions of fin materials on heat flow rate, temperature distribution, and effectiveness of fin truncated with cone shape. These numerical and analytical methods have been effectively applied to study the solutions of linear and nonlinear stiff problems. But besides their advantages, these techniques have several limitations. The finite difference (FD) methods are intuitive and easy to implement for simple problems. However, FDM may easily run into a problem while handling curved/ moving boundaries, complicated domains, unstructured grid and multiple disjoint manifolds within a problem. On the other hand, the requirement of a small parameter is the most significant drawback that is associated with the perturbation methods. Sometimes the small parameter may also be artificially introduced into the equations. The solutions, therefore, have a limited range of validity (Şenol et al. 2013). Also, numerical solvers such as the Runge–Kutta methods are a family of iterative methods used by several researchers to approximate the solutions to a variety of differential equations. Such methods use discretization to calculate the solutions in small steps. Runge-Kutta methods have several drawbacks, the most notable of which are that they demand a substantial amount of additional computer time compared to multi-step approaches of equivalent accuracy and that they do not readily produce reliable global estimates of the truncation error.

In addition, since the 1950s, there has been substantial development of gradient-based techniques, and today there are multiple excellent options available for dealing with smooth nonlinear issues. These approaches only converge to a local minimum point for the objective function since the search process that they employ uses only local information (functions and their gradients at a place) (Dalla et al. 2021). The gradient-based methods estimate the motion by analysis of the strong differences in brightness between analyzed regions. The disadvantage of such approaches is the dependence on noise, occlusions, and discontinuity of the function (Starostenko et al. 2005).When traversing a parameter space using gradient-based approaches, there is a significant risk that the algorithm will become mired in a local minimum or maximum (s). This is due to the fact that the gradient is always zero at any local minima or maxima. To overcome these drawbacks, direct search and gradient free techniques are designed that are currently used for solving complex multidisciplinary design optimization problems (Talgorn et al. 2017; Alarie et al. 2021; Audet and Hare 2017). The algorithmic global convergence property of mesh adaptive direct search, supported by mathematical proof, makes it outperform heuristics in blackbox optimization as there is no guarantee/proof that heuristics will not converge to a non-minimizer (Audet 2014; Audet et al. 2022a). Mesh adaptive direct search is recommended to be used in blackbox optimization specially in the case of unreliable approximation of gradients (Audet et al. 2022b). So, in recent times researchers have focused their attention on developing artificial neural networks based evolutionary gradient-free techniques that do not require prior information about the problem. It is becoming more standard practise to use evolutionary computing as a method for resolving challenging real-world problems in fields such as industry, health, and the defence sector (Erdal et al. 2011; Tejani et al. 2018; Saka et al. 2016). The special advantages include the processes' flexibility and their capacity to self-adapt on the fly in order to search for optimal solutions (Aydoğdu et al. 2016; Tejani et al. 2019b; Aydoğdu and Saka 2012; Yousif and Saka 2021).

In this study, we have developed and implanted an intelligent technique based on metaheuristic approach (Tejani et al. 2021; Kumar et al. 2021b) of global and local search mechanism to study the temperature distribution in conductive-convective-radiative moving rod. Nowadays, metaheuristic optimization algorithms have turned out to be quite attractive because of their distinct advantages over traditional algorithms. They can be easily hybridized and broadly implemented to any complex problem that can be formulated as optimization problem. For the purpose of solving optimization issues, the metaheuristic algorithms have been selected because of their ease of use, simplicity, ability to avoid reaching a local optimal solution, and adaptability to a diverse set of challenges originating from a variety of academic fields. In recent years, nature-inspired, human-inspired and biological-inspired meta-heuristic optimizers have gained the attention of researchers. Some

recently developed meta-heuristic techniques include artificial hummingbird algorithm (AHA) (Zhao et al. 2022), sooty tern optimization algorithm (STOA) (Dhiman and Kaur 2019; He et al. 2022), multi-objective plasma generation optimizer (MOPGO) (Kumar et al. 2021a), dynastic optimization algorithm (DOA) (Wagan et al. 2020), Tiki-Taka algorithm (TTA) (Rashid 2020), color harmony algorithm (CHA) (Zaeimi and Ghoddosian 2020), arithmetic optimization algorithm (AOA) (Abualigah et al. 2021). Also, the hybridized stochastic methodologies have been used by researchers to study the variety of problems arising in various domain of optimization (Kumar et al. 2021c), thermal engineering (Khan et al. 2022b; Zhu et al. 2021; Khan et al. 2022a), civil engineering (Huang et al. 2021; Nguyen et al. 2021; Singh et al. 2022; Cui et al. 2021), computational chemistry (Khan et al. 2021e, 2021a), and fluid dynamics (Khan et al. 2021b; Tahani et al. 2016). These applications have motivated authors to extend and incorporated the computational strength of neural networks with hybridization of meta-heuristic techniques. The salient features of the proposed methodology are summarized as:

- This study analyzes the mathematical model of the moving hot rod subjected to convective and radiative environments with variable thermal conductivity and constant velocity. Further, an integrated soft computing technique based on the function approximating ability of artificial neural networks and the stochastic exploitation and exploration search strategies of arithmetic optimization algorithm and sequential quadratic optimization algorithms are utilized to construct the series solutions for different cases of the moving rod.
- The proposed FANN-AOA-SQP algorithm is implemented in an unsupervised manner to study the effect of variations in significant parameters such as ambient temperature, radiation-conduction number, Peclet number, nonconstant thermal conductivity, and initial temperature parameter on the temperature gradient of the rod.
- The results are validated by comparing the statistics with the numerical solutions by Runge-Kutta-Fehlberg method and other machine learning techniques. The accuracy of the solutions in further dictates by the values of absolute errors and performance measures. In addition, the proposed FANN-AOA-SQP algorithm is simple to put into practice because it only requires the basic settings for the parameters and sufficient termination condition before execution.
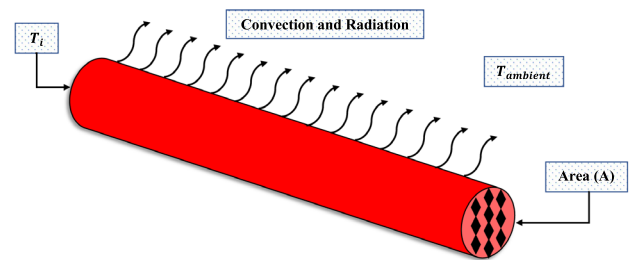

Fig. 1 Schematic view of the hot moving rod

2 Mathematical formulation

This study explores the heat transfer between the moving, convective and radiative hot rod with the surrounding. The rod of length L has a constant cross sectional area A, as illustrated in Fig. 1 is considered that emerges from a furnace or an intermediary heating station at a constant velocity of V. The initial temperature of the rod is T_i and is instantly exposed to ambient temperature denoted by $T_{ambient}$. It is assumed that T_i is greater than $T_{ambient}$ and that the rod's movement in the environment results in the formation of airflow at the rod's surface. In this scenario, both convection and radiation heat transfer is occurring simultaneously. Radiative heat transmission greatly influences the cooling process when there is no forced heat transfer, i.e., only the natural convective heat transfer occurs.

In addition to that, it is presumed that the rod is grey in colour, and the coefficient of emissivity is thought to remain unchanged. The swaying motion and rising temperature of the hot rod, as previously stated, provide a steady and consistent convective flow around the rod. As a result, the heat transfer coefficient, denoted by h, may be thought of as being constant over the rod's surface up to the end of the cooling process (Kundu and Yook 2021). The influence of temperature on thermal conductivity varies depending on whether the material is a metal or a nonmetal. Thermal conductivity in metals is mainly owing to the presence of free electrons. When the temperature of a pure metal is raised, the electrical conductivity of the metal drops. As a direct consequence of this, the thermal conductivity is very stable. When it comes to alloys, the amount by which electrical conductivity shifts is typically just a marginal one; hence, the increase in thermal conductivity is typically proportionate to the increase in temperature (Sheikholeslami and Ganji 2018). Mathematically, the relation between the temperature and conduction of heat transfer coefficient is defined as Fallah Najafabadi et al. (2021)

$$k = k_0\big(1 - \big(T_{ambient-T}\big)\omega\big), \tag{1}$$

here k_0 is the coefficient of heat transmission by conduction at the surrounding temperature, ω is variation coefficient of thermal conductivity, which may be positive or negative, and zero in the case when conduction heat transfer coefficient is constant. The heat transfer process of the rod begins when it is deposited into the environment. The initial unstable and fluctuating condition of heat transport is eliminated immediately, leaving behind a significant majority of the absorbed energy within the rod, with just a minimal amount of energy exiting the rod's surface via convection and radiation. In this work, the temperature distribution of the rod is investigated under steady-state conditions. Furthermore, the radiation is only being emitted from the surface of the moving rod and into the surrounding environment, and since the rod is not receiving any substantial radiation from the surrounding environment, fluctuating radiation sink temperature may be ignored. The only direction in which heat is transferred is the x-direction, the airflow in the environment around the rod is laminar and consistent, and the rod does not experience any volumetric or longitudinal expansion while this process is taking place. The energy equation of the rod with convective and radiative heat transfer moving with constant speed is given as

$$\frac{d}{dx}\left(\left[1 + \omega\left(T - T_{ambient}\right)\right]\frac{dT}{dx}\right)$$
$$- \frac{hp}{k_0 A}\left(T - T_{ambient}\right) - \frac{\varepsilon\sigma p}{k_0 A}\left(T^4 - T_{ambient}^4\right) - \frac{1}{\alpha}V\frac{dT}{dx} = 0, \tag{2}$$

here T is the temperature of the rod, σ is density, $\alpha = k_0/\rho c$ is thermal diffusivity, ϵ is Stefan-Boltzmann constant and c is the specific heat capacity. Following dimensionless parameters are define to solve 2.

$$\lambda = \frac{T_{ambient}}{T_l}, \Theta = \frac{T}{T_i}, \eta = \frac{xL^*}{A}, L^* = \frac{pL}{A}, \tag{3}$$

here L denotes the length of the rod and p represents the circumference. Using dimensionless variables in Eq. (2) will result in following differential equation as Fallah Najafabadi et al. (2021)

$$\frac{d}{d\eta}\left(\left[1 + \gamma(\Theta - \lambda)\right]\frac{d\Theta}{d\eta}\right) - N_c(\Theta - \lambda)$$
$$- N_r\left(\Theta^4 - \lambda^4\right) - Pe\frac{d\Theta}{d\eta} = 0, \tag{4}$$

subjected to the boundary conditions which are defined as

$$\text{at} \quad \eta = 0, \quad \Theta = 1,$$
$$\text{at} \quad \eta = L^*, \quad \frac{d\Theta}{d\eta} = 0, \tag{5}$$

where Pe is Peclet number that shows the dimensionless velocity profile of the moving rod, N_r, N_c is

radiative-conductive parameter, and γ is thermal conductivity. These parameters are defined as

$$N_c = \frac{hA}{pk_0}, \gamma = \omega T_l, Pe = \frac{VA}{\alpha p}, N_r = \frac{\varepsilon\sigma T_l^3}{pk_0}. \tag{6}$$

3 Design methodology

In this section, the detailed procedure of the proposed soft computing algorithm i.e. FANN-AOA-SQP is presented that is based on the two phases. Initially, an unsupervised fitness function is constructed with FANN modeling in sense of mean square error. Further, the optimization procedures based on the global search ability of arithmetic optimization algorithm and local search mechanism of sequential quadratic programming are hybridized to optimize the neurons in FANN structure for the series solution of the nonlinear temperature distribution model of moving hot rod.

3.1 FANN modeling

The mathematical modeling of the feedforward artificial neural networks for solving the governing model in Eqs. (4), (5) is presented in this section. The approximate solution of the problem $\hat{\Theta}(\eta)$ in the form of continuous mapping of FANN with log-sigmoid ($J(\eta) = (1 + \exp(-\eta))^{-1}$) is given as

$$\hat{\Theta}(\eta) = \sum_{i=1}^{k} \tilde{a}_i J\left(\tilde{w}_i\eta + \tilde{b}_i\right) = \sum_{i=1}^{k} \frac{\tilde{a}_i}{\left(1 + e^{-(\tilde{w}_i\eta + \tilde{b}_i)}\right)}, \tag{7}$$

first and second order continuous derivatives of Eq. (7) are defined as

$$\frac{d\hat{\Theta}}{d\eta} = \sum_{i=1}^{k} \tilde{a}_i \frac{d}{d\eta}J\left(\tilde{w}_i\eta + \tilde{b}_i\right)$$
$$= \sum_{i=1}^{k} \frac{\tilde{a}_i\tilde{w}_i e^{-(\tilde{w}_i\eta + \tilde{b}_i)}}{\left(1 + e^{-(\tilde{w}_i\eta + \tilde{b}_i)}\right)^2}, \tag{8}$$

$$\frac{d^2\hat{\Theta}}{d\eta^2} = \sum_{i=1}^{k} \tilde{a}_i \frac{d^2}{d\eta^2}J\left(\tilde{w}_i\eta + \tilde{b}_i\right)$$
$$= \sum_{i=1}^{k} \tilde{a}_i\tilde{w}_i^2\left(\frac{2e^{-2(\tilde{w}_i\eta + \tilde{b}_i)}}{\left(1 + e^{-(\tilde{w}_i\eta + \tilde{b}_i)}\right)^3} - \frac{e^{-(\tilde{w}_i\eta + \tilde{b}_i)}}{\left(1 + e^{-(\tilde{w}_i\eta + \tilde{b}_i)}\right)^2}\right), \tag{9}$$

where $\tilde{a} = [\tilde{a}_1, \tilde{a}_2, \tilde{a}_3, \ldots, \tilde{a}_k], \tilde{b} = [\tilde{b}_1, \tilde{b}_2, \tilde{b}_3, \ldots, \tilde{b}_k]$ and $\tilde{c} = [\tilde{c}_1, \tilde{c}_2, \tilde{c}_3, \ldots, \tilde{c}_k]$ are the unknown neurons in FANN

structure that are to be found during the optimization procedure of the unsupervised fitness function which is defined as

$$E_{Fit} = E_{Fit-1} + E_{Fit-2}, \tag{10}$$

where E_{Fit-1} and E_{Fit-2} are associated to the ANN models of differential equation and the boundary conditions which are given as

$$E_{Fit-1} = \frac{1}{N} \sum_{m=1}^{N} \left(\frac{d}{d\eta_m} \left([1 + \gamma(\Theta_m - \lambda)] \frac{d\Theta_m}{d\eta_m} \right) - N_c(\Theta_m - \lambda) - N_r(\Theta_m^4 - \lambda^4) - Pe \frac{d\Theta_m}{d\eta_m} \right), \tag{11}$$

$$E_{Fit-2} = \frac{1}{2} \left(\hat{\Theta}(1) - 1 \right)^2 + \frac{1}{2} \left(\frac{d\hat{\Theta}}{d\eta}(L^*) - 0 \right)^2. \tag{12}$$

where $Nh = 1, \Theta_m = \Theta(\eta_m)$, and $\eta_m = mh$. The FANN structure for the governing model of moving rod interms of input, hidden and output layers is shown through Fig. 2.

3.2 Optimization procedure

This section, explains the optimization process of the FANN weights in fitness function by operating the integrated strength of meta-heuristic computing process based on AOA supported with local search strategy of SQP.

Arithmetic optimization algorithm (AOA) is meta-heuristic technique which is inspired by the application of basic mathematical operators such as addition (A), subtraction (S), multiplication (M), and division (D) in searching the optimal solution for mathematical optimization problems (Abualigah et al. 2021). Since, AOA is population-based gradient-free algorithm so initially, it generates the set of random solutions as given in Eq. (13)

$$X = \begin{bmatrix} x_{1,1} & \cdots & \cdots & x_{1,j} & x_{1,n-1} & x_{1,n} \\ x_{2,1} & \cdots & \cdots & x_{2,j} & \cdots & x_{2,n} \\ \cdots & \cdots & \cdots & \cdots & \cdots & \cdots \\ \vdots & \vdots & \vdots & \vdots & \vdots & \vdots \\ x_{N-1,1} & \cdots & \cdots & x_{N-1,j} & \cdots & x_{N-1,n} \\ x_{N,1} & \cdots & \cdots & x_{N,j} & x_{N,n-1} & x_{N,n} \end{bmatrix} \tag{13}$$

Following the initialization process, the search phases of exploration and exploitation are selected based on a function known as the Math Optimizer Accelerated (MOA) which is defined as
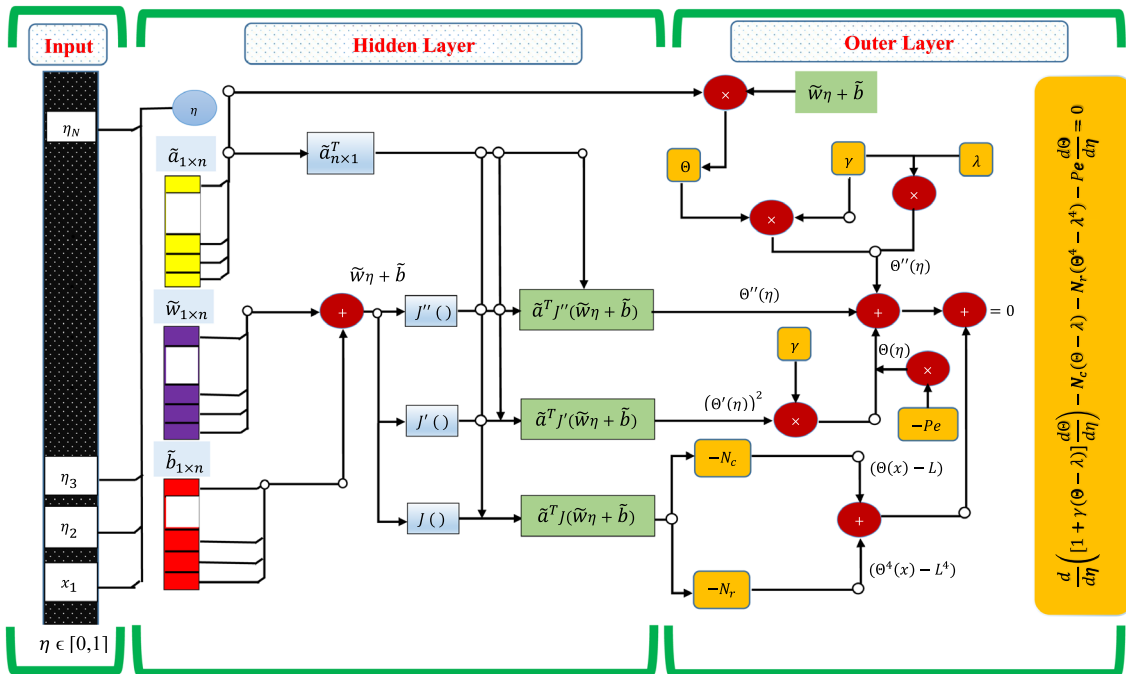
Fig. 2 Construction of FANN architecture for mathematical model of convective, radiative and moving rod

$$\text{MOA}(t_c)$$
$$= \text{Min} + t_c \times \left(\frac{\text{Max} - \text{Min}}{t_M} \right), \tag{14}$$

here t_c and T_M are current and maximum iteration. Max and min represents the MAXIMUM accelerated values of MOA. The exploration phase is conditioned by MOA when $r1 > MOA$, where $r1$ is a random number. The mathematical

Fig. 3 Model for repositioning math operators in AOA in the direction of the optimum solution (Abualigah et al. 2021)

model for the search strategy of multiplication and division in exploration phase in modeled as

$$x_{i,j}(t_c + 1)$$
$$= \begin{cases} \text{best}\,(x_j) \times \text{MOP} \times \big((\text{UB}_j - \text{LB}_j) \times \mu + \text{LB}_j\big), & \text{for } r_2 \quad gt; 0.5 \\ \text{best}\,(x_j) \div (\text{MOP} + \varepsilon) \times \big((\text{UB}_j - \text{LB}_j) \times \mu + \text{LB}_j\big), & \text{for } r_2 \quad lt; 0.5 \end{cases} \tag{15}$$

where ε is constant (small integer), $x_{i,j}(t_c + 1)$, represents the solution and at ith iteration, best (x_j) shows the best so far solution, LB_j, UB_j are lower and upper bounds of jth position, and μ is the controlling parameter to adjust the search process of this phase. To control the range of the candidate solution in AOA, another function known as Math Optimizer Probability (MOP) is defined given in Eq. (16).

$$\text{MOP}(t_c) = 1 - \frac{(t_c)^{1/\alpha}}{(t_M)^{1/\alpha}}, \tag{16}$$

here α is sensitive parameter that reflects the search through the iteration. In second phase, the arithmetic operators such as addition and subtraction are incorporated to update the position of the candidate solution and achieve the optimum solution. The searching methodology of different operators towards the optimal solution is shown through Fig. 3. Mathematically, the exploitation phase is modeled as

Fig. 4 Working mechanism of the proposed technique

$$x_{i,j}(t_c + 1)$$
$$= \begin{cases} \text{best}(x_j) - \text{MOP} \times \left[(\text{UB}_j - \text{LB}_j) \times \mu + \text{LB}_j\right], & r_3 < 0.5 \\ \text{best}(x_j) + \text{MOP} \times \left[(\text{UB}_j - \text{LB}_j) \times \mu + \text{LB}_j\right], & \text{otherwise} \end{cases}$$
$$\tag{17}$$

the decision on whether to execute A or S is made based on the value of r3. When $r3$ is more than 0.5, the addition operator is performed and the subtraction operator is ignored until the A completes the task, however when $r3$ is less than 0.5 then viceversa occurs. The detailed flow chart of the working mechanism of AOA is shown in Fig. 4.
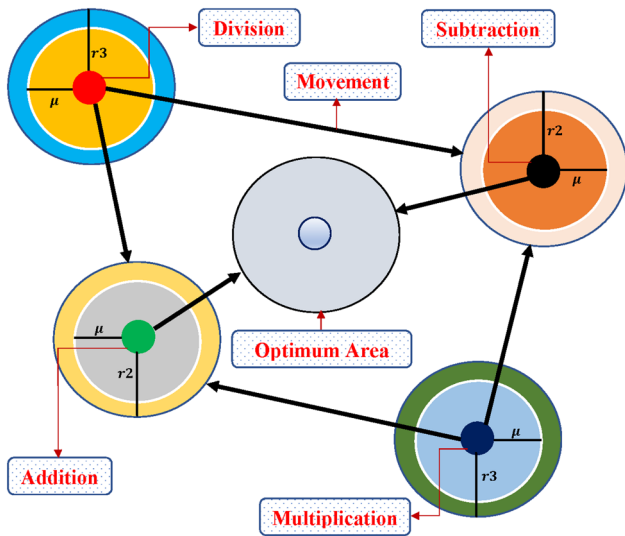
3.2.1 The proposed FANN-AOA-SQP algorithm

Metaheuristic algorithms (MA) are a class of high-level strategies or heuristics that are used to find, or generate a sufficiently good solution to optimization problems encountered in a various applications of applied physics and mathematics.The AOA algorithm is a metahierarchical one, and its drawbacks include poor exploration capabilities and a high propensity to settle for local optimal solutions. In order, to encounter this drawback, the designed variable of FANNs initially with AOA are fed into sequential quadratic programming for rapid local convergence. SQP is a prominent local search method which has been effectively used for solving constrained and unconstrained optimization problems with low dimensions. Some recent application of SQP includes the prediction of powertrain torque and vehicle speed (Yang et al. 2021), cost minimization of a hybrid photovoltaic, diesel generator, and battery energy storage system (Tian et al. 2021), dynamic combined economic emission dispatch problem (Gul et al. 2021), robust design of power system stabilizers and static VAR compensator (Welhazi et al. 2022), and transient control of turbofan engines (Wang et al. 2021).

4 Numerical experimentation and discussion

In this section, the proposed methodology (FANN-AOA-SQP) is implemented on the nonlinear governing model of the convective, radiative, and moving rod to study the influence of the variation in different parameters (ambient temperature, radiation-conduction number, Peclet number, nonconstant thermal conductivity, and initial temperature parameter) on the temperature distribution of the rod. An overview of the problem and different cases based on variations of the parameters are shown in Fig. 5.

The fitness function given in Eqs (10)–(12) are optimized using the design strength of the FANN-AOA-SQP algorithm to calculate the approximate solutions. The comparison of the statistics, showing the results for the temperature distribution in moving fin for $N_c = N_r = 4, \lambda = 0.2, Pe = 3$ and $\gamma = 0.2$ obtained by proposed algorithm are compared with radial basis function approximation method (RBFM)

Fig. 5 An overview of the problem and different cases based on changes in physical parameters

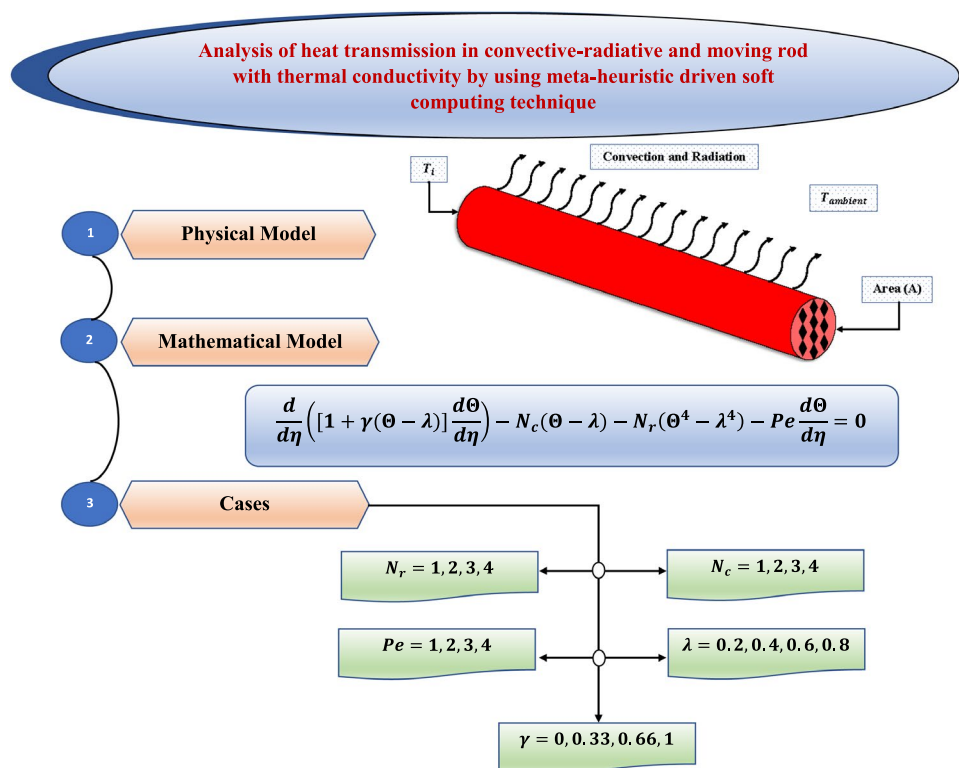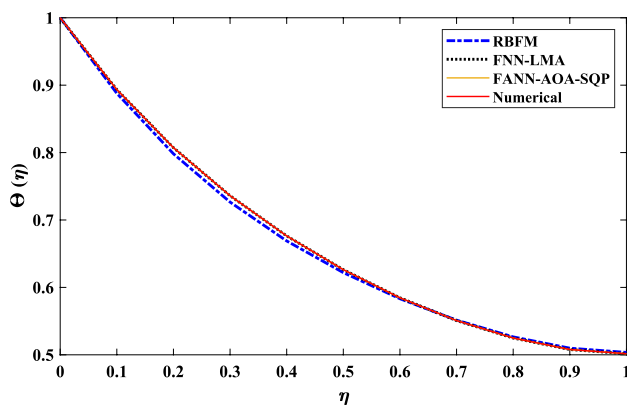**Table 1** Comparison of results with radial basis function approximation method (RBFM), Runge–Kutta–Fehlberg method, and machine-learning technique such as FNN and Levenberg–Marquardt algorithm

η	Solution				Absolute errors		
	RBFM	FNN-LM	FANN-AOA-SQP	RKFM	RBFM	FNN-LM	FANN-AOA-SQP
0.0	1.00004711	0.99966884	0.99999695	1.00000000	4.71082000E−05	3.31156169E−04	3.04890500E−06
0.1	0.88790222	0.89345397	0.89345652	0.89345656	5.55433579E−03	2.58674300E−06	3.27940001E−08
0.2	0.79822750	0.80727280	0.80726970	0.80726900	9.04150754E−03	3.79515600E−06	6.94919000E−07
0.3	0.72657971	0.73601715	0.73601418	0.73601461	9.43490678E−03	2.54011300E−06	4.37278000E−07
0.4	0.66892546	0.67638540	0.67638294	0.67638277	7.45730466E−03	2.62952900E−06	1.67581000E−07
0.5	0.62192928	0.62632454	0.62632199	0.62632195	4.39267235E−03	2.58619100E−06	3.52539999E−08
0.6	0.58319320	0.58462419	0.58462424	0.58462484	1.43163246E−03	6.47788000E−07	5.92566000E−07
0.7	0.55143395	0.55076746	0.55076317	0.55076305	6.70892909E−04	4.40778900E−06	1.15908000E−07
0.8	0.52658713	0.52486976	0.52487350	0.52487436	1.71277349E−03	4.59367100E−06	8.53268000E−07
0.9	0.50983228	0.50786431	0.50786057	0.50786072	1.97156193E−03	3.58925000E−06	1.47996000E−07
1.0	0.50353693	0.50158037	0.50158039	0.50158037	1.95655685E−03	1.74000037E−10	1.10550000E−08

(a) Approximate Solution
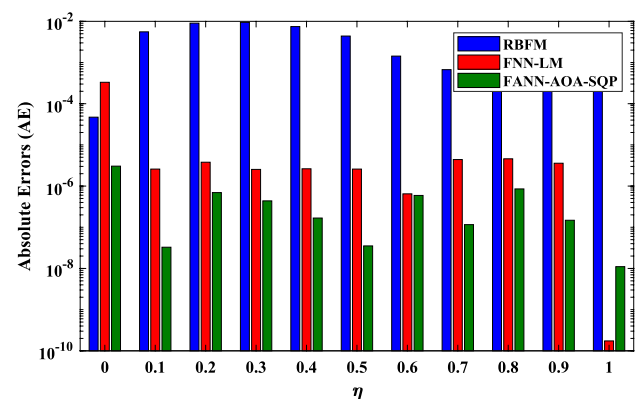
(b) Absolute Errors

Fig. 6 a, **b** Illustrates the comparison of solutions and absolute errors in temperature distribution of the moving rod with $N_c = N_r = 4, \lambda = 0.2, Pe = 3$ and $\gamma = 0.2$

(Fallah Najafabadi et al. 2021), Runge-Kutta-Fehlberg method and machine learning algorithm such as FNN and Levenberg–Marquardt algorithm (Hsiang et al. 2020) as dictated in Table 1. Figure 6 illustrates the solutions' accuracy compared to the state-of-the-art techniques. It is observed that results by the FANN-AOA-SQP algorithm overlap the numerical solution with absolute minimum errors that lie between 10^{-6} to 10^{-8}.

The influence of physical parameters ($N_r, Pe, \lambda, N_c, \gamma$) on temperature distribution Θ of the moving hot rod are dictated in Tables 2, 3, 4 and 5 and graphically demonstrated through Fig. 7. It is observed from Fig. 7a and b that the temperature distribution of the rod in the passive device reduces when the conductive-convective parameter increases, implying that the pace at which heat is transferred via the fin is increased, and as a result, the efficiency with which the fin transfers heat is enhanced. This is due to the fact that convective heat

transfer occurs when the temperature rises, convective cooling becomes more effective, lowering the fin's temperatures. By extension, a reduction in the value of the fin efficiency is produced by increasing the value of the convective-conductive parameter. In addition, the influence in Peclet number is shown through Fig. 7c. The values of the temperature distribution in the fin rise in proportion to the increase in the Peclet number. This is expected because, as the Peclet number increases, the material moves faster, and the time during which the material is exposed to the environment shortens. Additionally, the heat loss from the fin surface becomes stronger, increasing the temperature of the fin surface. Figure 7d depicts the effect of ambient temperature on the thermal performance of the heat exchanger. The greater the dimensionless ambient temperature, the higher the temperature in the surrounding area. As a result, heat transfer from the fin surface to the surrounding environment is reduced. So,
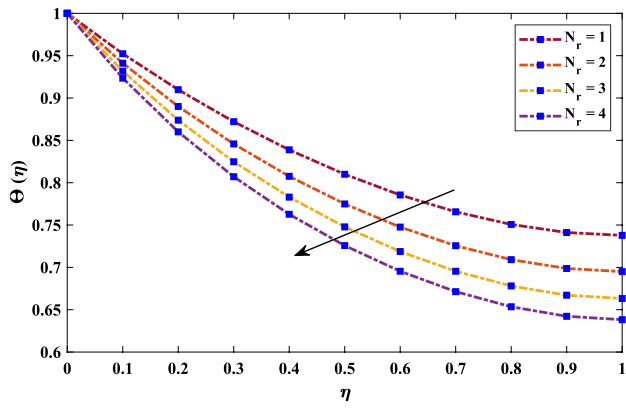
(a) Variations in radiation parameter.
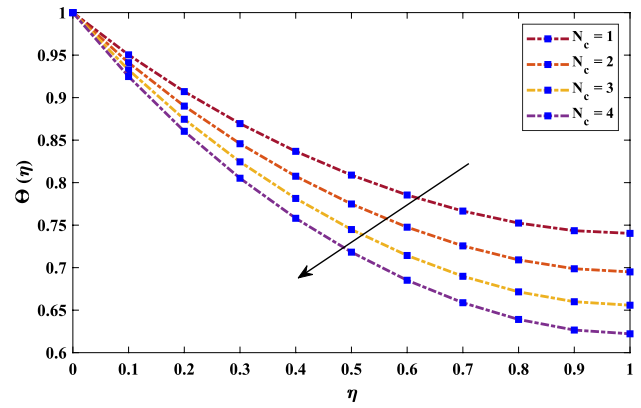
(b) Variations in conduction parameter
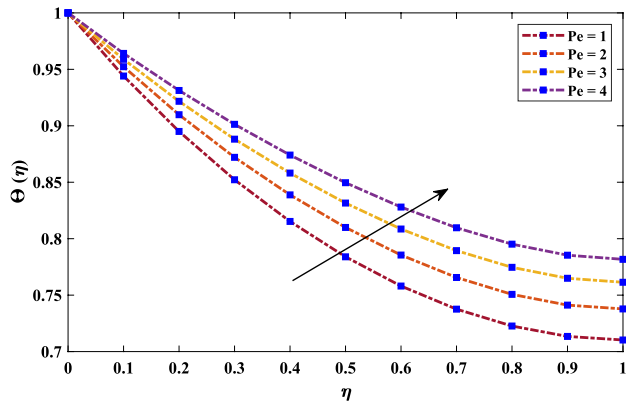
(c) Variations in Peclet number
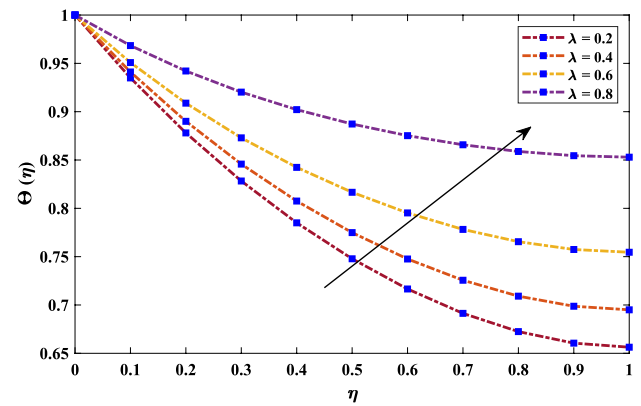
(d) Variations in nondimensional ambient temperature.
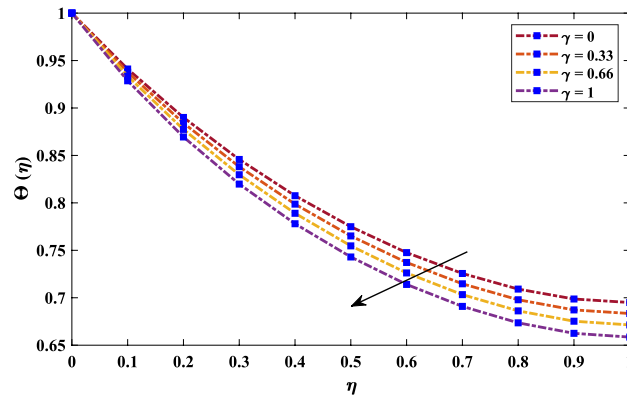
(e) Variations in nonconstant thermal conductivity and initial temperature parameter.

Fig. 7 Illustration of influence due to changes in different physical parameters on the temperature distribution of the moving fin with **a** $\lambda = 0.4, \gamma = 1, N_c = 2, Pe = 2$, **b** $\gamma = 1, \lambda = 0.4, N_r = N_c = 2$, **c** $Pe = 2, \gamma = 1, N_r = N_c = 2$, **d** $\gamma = 1, \lambda = 0.4, Pe = 2, N_r = 2$, and **e** $N_r = N_c = 2, \lambda = 0.4, Pe = 2$
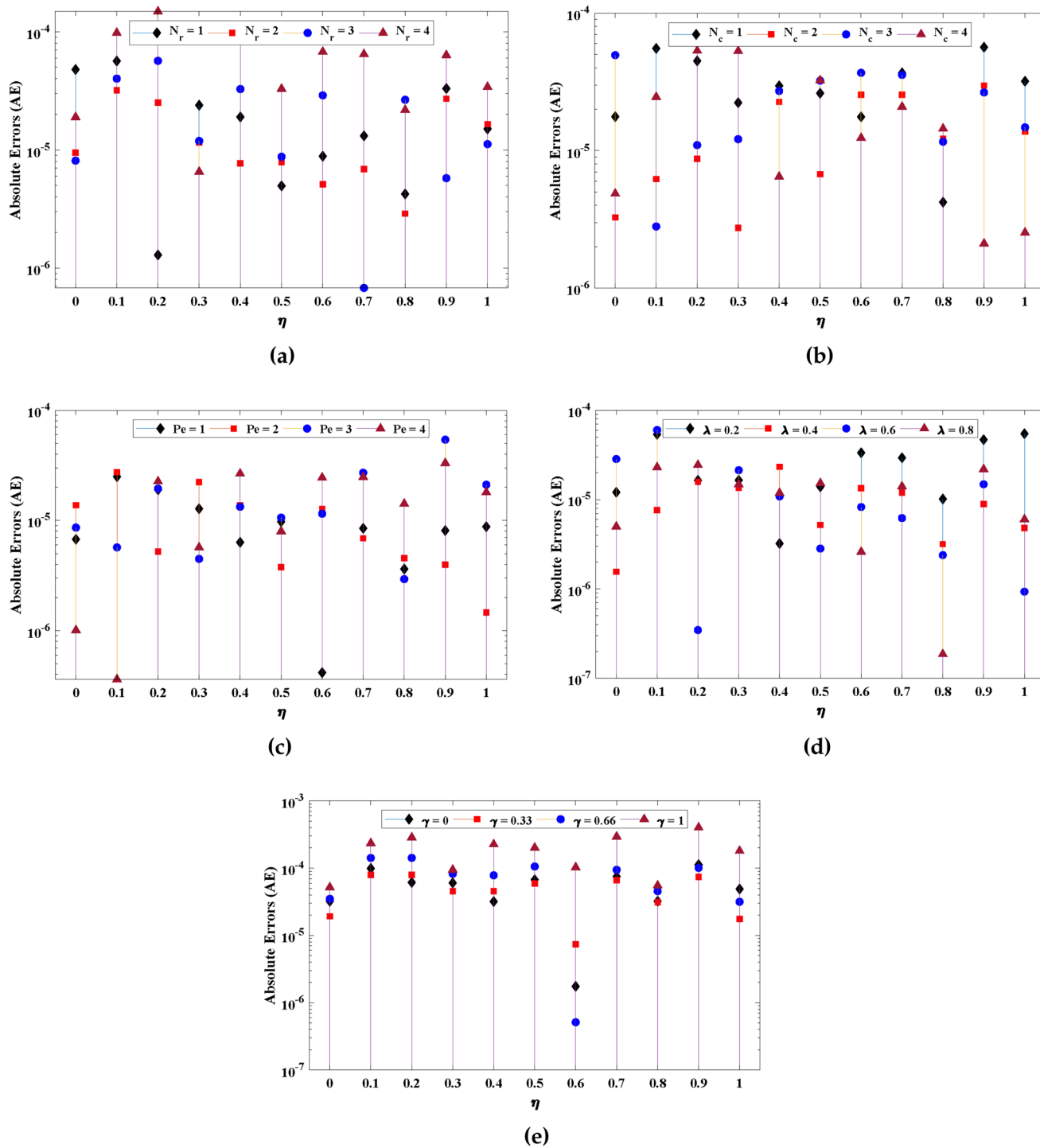
Fig. 8 Illustration of the absolute errors in the solutions of FANN-AOA-SQP algorithm for different cases of Eq. (4) with **a** $\lambda = 0.4, \gamma = 1, N_c = 2, Pe = 2$, **b** $\gamma = 1, \lambda = 0.4, N_r = N_c = 2$, **c** $Pe = 2, \gamma = 1, N_r = N_c = 2$, **d** $\gamma = 1, \lambda = 0.4, Pe = 2, N_r = 2$, and **e** $N_r = N_c = 2, \lambda = 0.4, Pe = 2$

more the ambient temperature less will be the transfer of heat. Further, Fig. 8 is plotted to demonstrate the accuracy of the approximate solutions obtained by the proposed algorithm for different cases of the moving rod. The approximate solution for different cases can be generated by using the equations given in "Appendix".

(a) $Pe = 2, \gamma = 1, \lambda = 0.4$ and $\eta = 1$ **(b)** $N_c = 2, \gamma = 1, \lambda = 0.4$ and $\eta = 1$
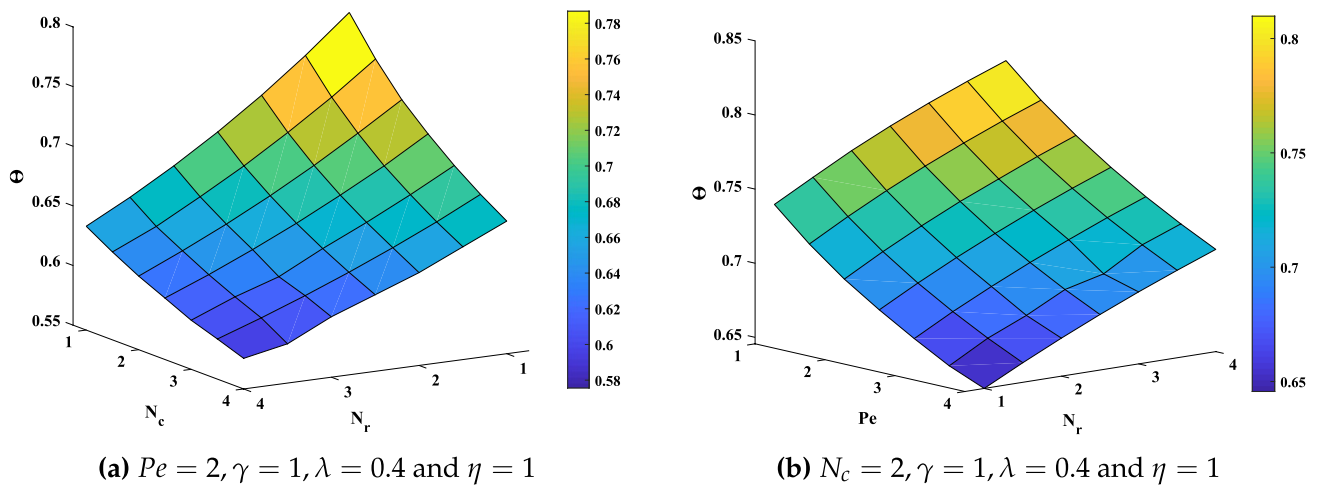
Fig. 9 **a**, **b** Shows the combine effects of N_c, N_r and Pe on the temperature performance of the rod

Table 2 Statistics of the calculated results for thermal distribution of a wetted porous structure and their corresponding AE obtained by the proposed scheme for variations in radiations parameter with $N_c = 2, \gamma = 1, \lambda = 0.4$ and $Pe = 2$

	Solutions				Absolute errors			
	$N_r = 1$	$N_r = 2$	$N_r = 3$	$N_r = 4$	$N_r = 1$	$N_r = 2$	$N_r = 3$	$N_r = 4$
0.0	0.999993	1	0.999999	0.999998	4.786643E−05	9.468818E−06	8.100852E−06	1.890666E−05
0.1	0.95232	0.941093	0.931675	0.923461	5.650062E−05	3.186095E−05	4.012722E−05	9.771750E−05
0.2	0.909807	0.890034	0.873857	0.86004	1.288105E−06	2.510250E−05	5.673190E−05	1.483477E−04
0.3	0.872055	0.845764	0.824718	0.80706	2.384707E−05	1.156753E−05	1.190149E−05	6.518979E−06
0.4	0.838808	0.807543	0.782985	0.7627	1.900344E−05	7.672769E−06	3.270042E−05	1.068978E−04
0.5	0.809949	0.774896	0.74781	0.725736	4.957698E−06	7.871931E−06	8.748966E−06	3.284028E−05
0.6	0.785501	0.747583	0.718686	0.695405	8.825988E−06	5.125001E−06	2.893456E−05	6.756444E−05
0.7	0.765634	0.725591	0.695413	0.671328	1.313187E−05	6.859307E−06	6.777202E−07	6.451270E−05
0.8	0.750683	0.70914	0.678091	0.653485	4.233063E−06	2.881823E−06	2.655502E−05	2.175318E−05
0.9	0.741163	0.698696	0.667123	0.642213	3.302314E−05	2.712731E−05	5.753817E−06	6.329484E−05
1.0	0.737794	0.695	0.663244	0.638229	1.503751E−05	1.651211E−05	1.118278E−05	3.405407E−05

Table 3 The statistical analysis of the approximated solutions and magnitude of the errors in the results by the designed paradigm for variations in conduction parameter with $N_r = 2, \gamma = 1, \lambda = 0.4$ and $Pe = 2$

	Solutions				Absolute errors			
	$N_c = 1$	$N_c = 2$	$N_c = 3$	$N_c = 4$	$N_c = 1$	$N_c = 2$	$N_c = 3$	$N_c = 4$
0.0	0.999998	0.999999	1.000015	0.999999	1.765931E−05	3.267390E−06	4.948946E−05	4.863930E−06
0.1	0.950335	0.941092	0.932628	0.924799	5.538637E−05	6.221897E−06	2.806658E−06	2.454132E−05
0.2	0.907085	0.890033	0.874545	0.860391	4.491420E−05	8.717667E−06	1.097204E−05	5.322621E−05
0.3	0.869432	0.845763	0.824453	0.805191	2.231986E−05	2.739705E−06	1.212480E−05	5.298644E−05
0.4	0.836810	0.807543	0.781420	0.758063	2.959437E−05	2.261680E−05	2.715352E−05	6.466197E−06
0.5	0.808868	0.774896	0.744826	0.718218	2.612840E−05	6.753803E−06	3.227777E−05	3.240068E−05
0.6	0.785445	0.747583	0.714324	0.685176	1.760557E−05	2.547717E−05	3.681993E−05	1.236171E−05
0.7	0.766565	0.725591	0.689832	0.658754	3.673281E−05	2.548095E−05	3.551765E−05	2.083964E−05
0.8	0.752438	0.709139	0.671538	0.639074	4.220622E−06	1.218358E−05	1.160764E−05	1.445326E−05
0.9	0.743477	0.698695	0.659927	0.626600	5.648190E−05	2.977799E−05	2.650398E−05	2.109202E−06
1.0	0.740312	0.695000	0.655815	0.622181	3.198311E−05	1.374518E−05	1.476485E−05	2.533932E−06

Table 4 Statistics of the calculated results for thermal distribution of a wetted porous structure and their corresponding AE obtained by the proposed scheme for variations in velocity parameter (Pe) with $N_r = N_c = 2, \gamma = 1$ and $\lambda = 0.4$

	Solutions				Absolute errors			
	$Pe = 1$	$Pe = 2$	$Pe = 3$	$Pe = 4$	$Pe = 1$	$Pe = 2$	$Pe = 3$	$Pe = 4$
0.0	1.000001	1.000002	0.999998	1.000000	6.750379E−06	1.377765E−05	8.626292E−06	1.009510E−06
0.1	0.944059	0.952329	0.958877	0.964115	2.496484E−05	2.751508E−05	5.697738E−06	3.616491E−07
0.2	0.894988	0.909815	0.921689	0.931282	1.900408E−05	5.224604E−06	1.945949E−05	2.259382E−05
0.3	0.852201	0.872061	0.888158	0.901300	1.276597E−05	2.228531E−05	4.481846E−06	5.690388E−06
0.4	0.815278	0.838813	0.858124	0.874065	6.334014E−06	1.374461E−05	1.330689E−05	2.661534E−05
0.5	0.783945	0.809953	0.831557	0.849588	9.743473E−06	3.771875E−06	1.060670E−05	7.969113E−06
0.6	0.758057	0.785504	0.808565	0.828014	4.160123E−07	1.272560E−05	1.151443E−05	2.447243E−05
0.7	0.737593	0.765636	0.789427	0.809677	8.486989E−06	6.885369E−06	2.709994E−05	2.477499E−05
0.8	0.722647	0.750683	0.774632	0.795156	3.624936E−06	4.562607E−06	2.938193E−06	1.417513E−05
0.9	0.713430	0.741162	0.764930	0.785372	8.102531E−06	3.977544E−06	5.407609E−05	3.315218E−05
1.0	0.710266	0.737792	0.761395	0.781709	8.774453E−06	1.461179E−06	2.111133E−05	1.798909E−05

Table 5 The statistical analysis of the approximated solutions and magnitude of the errors in the results by the designed paradigm for variations in λ with $N_r = N_c = Pe = 2$ and $\gamma = 1$

	Solutions				Absolute errors			
	$\lambda = 0.2$	$\lambda = 0.4$	$\lambda = 0.6$	$\lambda = 0.8$	$\lambda = 0.2$	$\lambda = 0.4$	$\lambda = 0.6$	$\lambda = 0.8$
0.0	1.000001	0.999997	0.999992	1.000003	1.206115E−05	1.554676E−06	2.844812E−05	4.983000E−06
0.1	0.934938	0.941091	0.950829	0.968400	5.368228E−05	7.637639E−06	6.012020E−05	2.300215E−05
0.2	0.878037	0.890031	0.908830	0.942108	1.643381E−05	1.581024E−05	3.458689E−07	2.440437E−05
0.3	0.828284	0.845761	0.872940	0.920246	1.648635E−05	1.346863E−05	2.132732E−05	1.478513E−05
0.4	0.785006	0.807541	0.842379	0.902131	3.217766E−06	2.324565E−05	1.082855E−05	1.185446E−05
0.5	0.747812	0.774894	0.816599	0.887242	1.390824E−05	5.198774E−06	2.826995E−06	1.522597E−05
0.6	0.716556	0.747582	0.795253	0.875201	3.337832E−05	1.344821E−05	8.252745E−06	2.595468E−06
0.7	0.691332	0.725590	0.778195	0.865767	2.932649E−05	1.193094E−05	6.203705E−06	1.401837E−05
0.8	0.672463	0.709138	0.765487	0.858839	1.014651E−05	3.174981E−06	2.388131E−06	1.857010E−07
0.9	0.660517	0.698693	0.757421	0.854476	4.681821E−05	8.897335E−06	1.482842E−05	2.186521E−05
1.0	0.656310	0.694998	0.754557	0.852929	5.464326E−05	4.818057E−06	9.302385E−07	6.008371E−06

The combined effect of different parameters on the temperature performance at the rod's tip is shown in Fig. 9. The three-dimensional surface plots show that temperature at the rod's tip is maximum when convective and radiative parameters are minimum, and Peclet number is maximum. It is further noticed that the effect of these critical parameters is nonlinear, reflecting the higher temperature dependency on N_c and N_r.

5 Performance measures

This section incorporates different performance measures to explore the efficiency, stability, and accuracy of the approximate solutions calculated by the proposed computational (FANN-AOA-SQP) algorithm. The performance indices are defined in terms of mean absolute deviations (MAD), Theil's

inequality coefficient (TIC), root mean square error (RMSE), and error in Nash–Sutcliffe Efficiency (ENSE). Mathematical relations for these indices are defined as Umar et al. (2020)

$$\text{MAD} = \frac{1}{M} \sum_{i=1}^{M} \left(\left| \hat{\Theta}(\eta_i) - \Theta(\eta_i) \right| \right), \tag{18}$$

$$\text{TIC} = \frac{\sqrt{\frac{1}{M} \sum_{i=1}^{M} \left(\hat{\Theta}(\eta_i) - \Theta(\eta_i) \right)^2}}{\sqrt{\frac{1}{M} \sum_{i=1}^{M} \left(\hat{\Theta}(\eta_i) \right)^2} + \sqrt{\frac{1}{M} \sum_{i=1}^{M} \left(\Theta(\eta_i) \right)^2}}, \tag{19}$$

$$\text{RMSE} = \sqrt{\frac{1}{M} \sum_{i=1}^{M} \left(\hat{\Theta}(\eta_i) - \Theta(\eta_i) \right)^2}, \tag{20}$$

$$ENSE = |1 - NSE|, \tag{21}$$

where NSE is Nash-Sutcliffe Efficiency and is defined as Umar et al. (2020); Khan et al. (2021a)

$$NSE = 1 - \left(\frac{\sum_{i=1}^{M} \left(\hat{\Theta}(\eta_i) - \Theta(\eta_i) \right)^2}{\sum_{i=1}^{M} \left(\Theta(\eta_i) - \frac{1}{M} \sum_{i=1}^{M} \left(\Theta(\eta_i) \right) \right)^2} \right). \tag{22}$$

here $\hat{\Theta}$ and Θ are the approximate and exact solutions for the problem. M corresponds to the total number of mesh (grid) points, and i denotes the number of current solution points. Since the FANN-AOA-SQP algorithm is an unsupervised learning strategy, it is important to use these performance indices to justify the accuracy of the solutions. For perfect modeling of approximate solutions, values of MAD, TIC, RMSE, and ENSE approach to zero.

To investigate the stability and durability of the results, the design method is executed for 100 times. The solution curves for the temperature distribution in the moving rod obtained during each run are plotted through Fig. 10. It is concluded that the approximate solutions for different cases overlap the numerical solution with 100% accuracy and stability. The behavior of fitness value and MAD of solution in each run is graphically shown through Fig. 11. The mean values of fitness function and MAD lies in the range of 10^{-5} to 10^{-6} and 10^{-4} to 10^{-5}, respectively. The detailed statistics of the performance indicators in terms of minimum value, mean and standard deviations are provided in Table 6. Clearly, it can be observed that for each case minimum values of fitness function, MAD, TIC, RMSE and ENSE lies between 10^{-8} to 10^{-9}, 10^{-6} to 10^{-7}, 10^{-4} to 10^{-5}, 10^{-5} to 10^{-6}, and 10^{-9} to 10^{-10} respectively. The global (average) values for each case lies around 10^{-4} to 10^{-6}. The results of ENSE are shown through the boxplots in Fig. 12. It can be seen that the upper quartile (maximum values) of boxplots for each case lie between 10^{-6} to 10^{-7}, which shows that the solutions of the proposed technique are accurate and stable. The normal distribution curves for the root mean
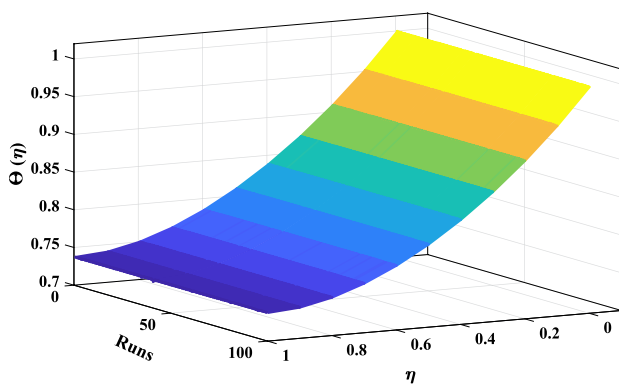
(a) $\lambda = 0.4, N_c = 2, N_r = 1, Pe = 2$ and $\gamma = 1$
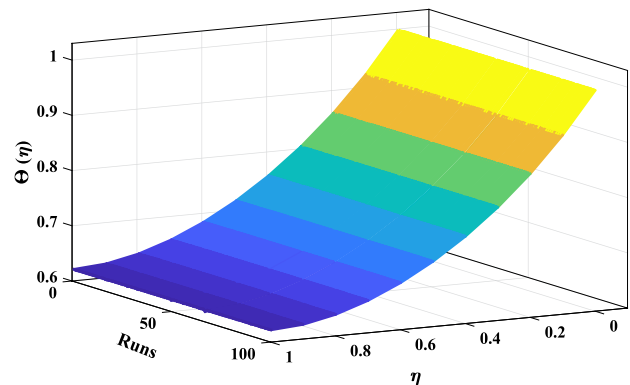
(b) $\lambda = 0.4, N_c = 1, N_r = 2, Pe = 4$ and $\gamma = 1$
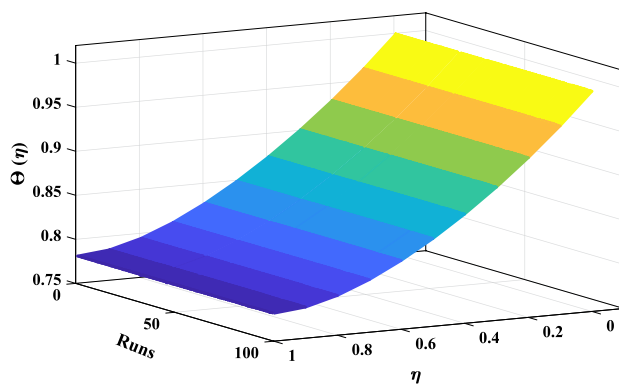
(c) $\lambda = 0.4, N_c = 2, N_r = 1, Pe = 4$ and $\gamma = 1$
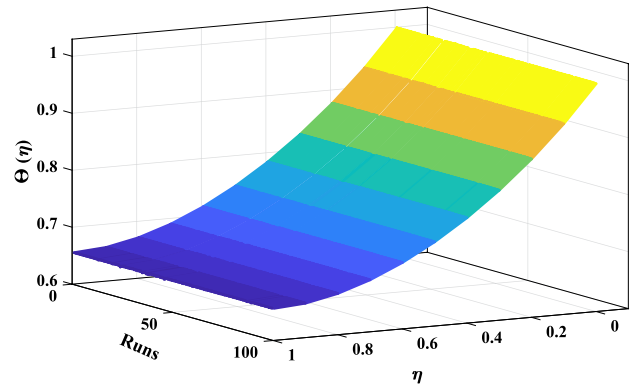
(d) $\lambda = 0.2, N_c = 2, N_r = 1, Pe = 2$ and $\gamma = 1$

Fig. 10 **a**, **b**, **c**, and **d** Approximate solution obtained by FANN-AOA-SQP algorithm in each run for different cases of moving rod
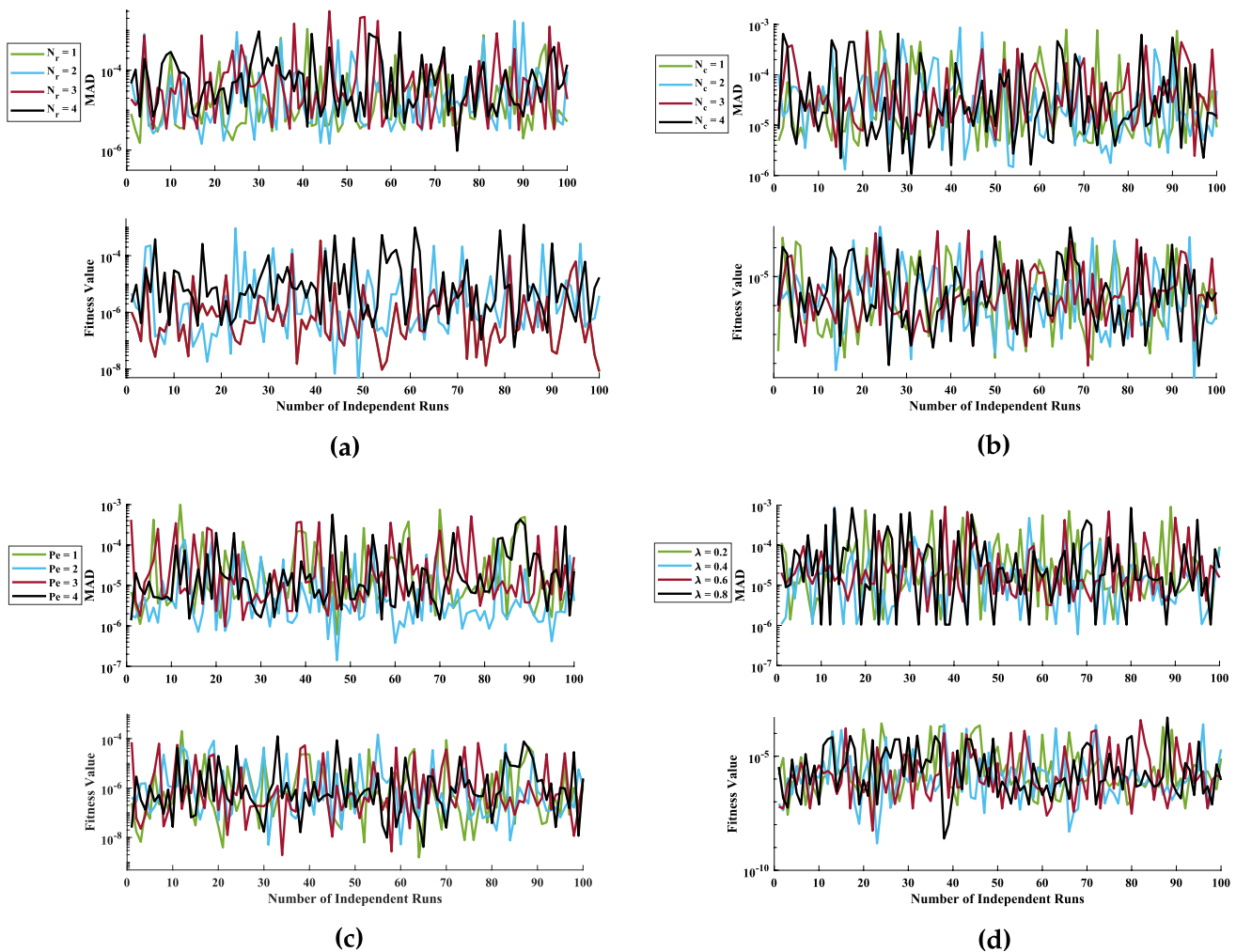
Fig. 11 **a**, **b**, **c**, and **d** Shows the behaviour of values of fitness function and mean absolute deviation by varying N_r, N_c, λ and Pe during 100 independent execution of the design algorithm

square error of the approximate solutions of moving rod with $\lambda = 0.2, Nr = Nr = 1, Pe = 2$ and $\gamma = 1$ are plotted through Fig. 13.

6 Conclusion

This paper investigates the thermal performance and heat transfer of the convective, radiative and moving rod with thermal conductivity by developing a met-heuristic driven approach based on the approximating computational ability of neural networks. Furthermore, the feedforward network is optimized by combining global and local search mechanisms such as Arithmetic optimization algorithm and sequential quadratic programming. The proposed FANN-AOA-SQP algorithm is implemented to study the rod's temperature distribution behavior by varying critical parameters (radiation parameter N_r, conduction parameter N_c, ambient temperature λ, Peclet number Pe and thermal conductivity γ). The results demonstrate that increase in N_c, Pe and N_r causes an increase in the temperature of the rod. In addition, the increase in velocity parameter (Pe) from 1 to 2 causes an increase in the temperature up to 7 to 10%.

Further, the design algorithm's accuracy, stability, and effectiveness are established by calculating the errors based on MAD, TIC, RMSE, ENSE, and AE. The values of these errors are approaching to zero, reflecting the perfect modeling of the solution compared to the other techniques available in the latest literature. The results and graphical analysis illustrate that the proposed approach is accurate and reliable in calculating solutions to complex real-world problems.

In the future, the author aims to extend the proposed meta-heuristic technique to solve high-dimensional problems, especially partial differential equations and fractional differential equations about complex problems such as epidemiology and population study, magnetic resonance

Table 6 Values of statistical operators for each case of the mathematical model of moving fin

Cases	Fitness function			MAD			TIC			RMSE			ENSE		
	Min.	Avg.	St. Div.	Min.	Avg.	St. Div.	Min.	Avg.	St. Div.	Min.	Avg.	St. Div.	Min.	Avg.	St. Div.
$N_r = 1$	8.12E−09	8.95E−06	3.75E−05	1.51E−06	5.96E−05	1.55E−04	4.75E−07	1.77E−05	4.61E−05	1.71E−06	6.38E−05	1.66E−04	3.39E−09	4.06E−05	2.03E−04
$N_r = 2$	3.08E−09	3.67E−05	1.12E−04	1.43E−06	1.04E−04	2.83E−04	5.13E−07	3.23E−05	8.58E−05	1.78E−06	1.12E−04	2.98E−04	2.28E−09	1.00E−04	4.47E−04
$N_r = 3$	7.88E−09	5.60E−05	1.38E−04	1.46E−06	1.95E−04	4.92E−04	5.94E−07	6.03E−05	1.49E−04	2.00E−06	2.03E−04	5.03E−04	1.97E−09	2.57E−04	1.07E−03
$N_r = 4$	5.88E−08	6.84E−05	1.95E−04	9.58E−07	1.21E−04	1.98E−04	3.84E−07	3.93E−05	6.39E−05	1.27E−06	1.30E−04	2.10E−04	7.41E−10	4.32E−05	1.32E−04
$N_c = 1$	1.33E−08	2.13E−05	4.51E−05	3.07E−06	8.49E−05	1.80E−04	1.05E−06	2.48E−05	5.12E−05	3.77E−06	8.92E−05	1.84E−04	1.45E−08	6.05E−05	1.98E−04
$N_c = 2$	3.21E−09	2.16E−05	6.78E−05	1.23E−06	6.90E−05	1.35E−04	3.75E−07	2.13E−05	4.02E−05	1.30E−06	7.40E−05	1.39E−04	1.68E−09	2.54E−05	1.05E−04
$N_c = 3$	8.34E−09	2.29E−05	6.73E−05	2.45E−06	7.94E−05	1.15E−04	9.75E−07	2.52E−05	3.52E−05	3.28E−06	8.47E−05	1.18E−04	5.25E−09	1.70E−05	5.14E−05
$N_c = 4$	8.17E−09	2.34E−05	6.45E−05	1.08E−06	8.94E−05	1.55E−04	3.91E−07	2.92E−05	4.92E−05	1.28E−06	9.53E−05	1.61E−04	8.52E−10	2.32E−05	6.37E−05
$P_e = 1$	1.56E−09	7.16E−06	2.31E−05	6.13E−07	6.90E−05	1.52E−04	2.05E−07	2.08E−05	4.59E−05	7.19E−07	7.30E−05	1.61E−04	4.61E−10	3.40E−05	1.45E−04
$P_e = 2$	1.92E−09	9.85E−05	9.12E−04	9.67E−07	6.11E−05	1.12E−04	2.89E−07	1.79E−05	3.21E−05	1.04E−06	6.46E−05	1.16E−04	1.39E−09	2.42E−05	6.52E−05
$P_e = 3$	5.05E−09	7.27E−06	1.96E−05	4.20E−07	4.91E−05	1.02E−04	1.41E−07	1.43E−05	2.88E−05	5.18E−07	5.25E−05	1.06E−04	3.17E−10	2.28E−05	7.52E−05
$P_e = 4$	4.15E−09	6.84E−06	1.84E−05	1.37E−06	4.66E−05	9.30E−05	3.91E−07	1.32E−05	2.54E−05	1.46E−06	4.94E−05	9.49E−05	4.02E−09	2.29E−05	8.51E−05
$\lambda = 0.2$	1.11E−08	2.55E−05	5.98E−05	1.40E−06	9.88E−05	1.96E−04	4.95E−07	3.12E−05	6.04E−05	1.67E−06	1.05E−04	2.03E−04	1.71E−09	4.18E−05	1.26E−04
$\lambda = 0.4$	1.50E−09	1.68E−05	5.02E−05	6.00E−07	4.01E−05	1.03E−04	2.15E−07	1.25E−05	3.05E−05	7.48E−07	4.35E−05	1.06E−04	4.01E−10	1.36E−05	9.21E−05
$\lambda = 0.6$	5.38E−09	1.71E−05	4.96E−05	2.20E−06	6.47E−05	1.47E−04	7.24E−07	1.92E−05	4.15E−05	2.63E−06	6.98E−05	1.51E−04	8.36E−09	4.42E−05	1.91E−04
$\lambda = 0.8$	2.46E−09	1.80E−05	5.34E−05	1.04E−06	1.06E−04	1.93E−04	3.47E−07	2.88E−05	5.13E−05	1.35E−06	1.12E−04	2.00E−04	5.34E−09	1.99E−04	6.04E−04

Fig. 12 **a**, **b**, **c**, and **d** Results of ENSE obtained by FANN-AOA-SQP algorithm during multiple runs for variations in critical parameters

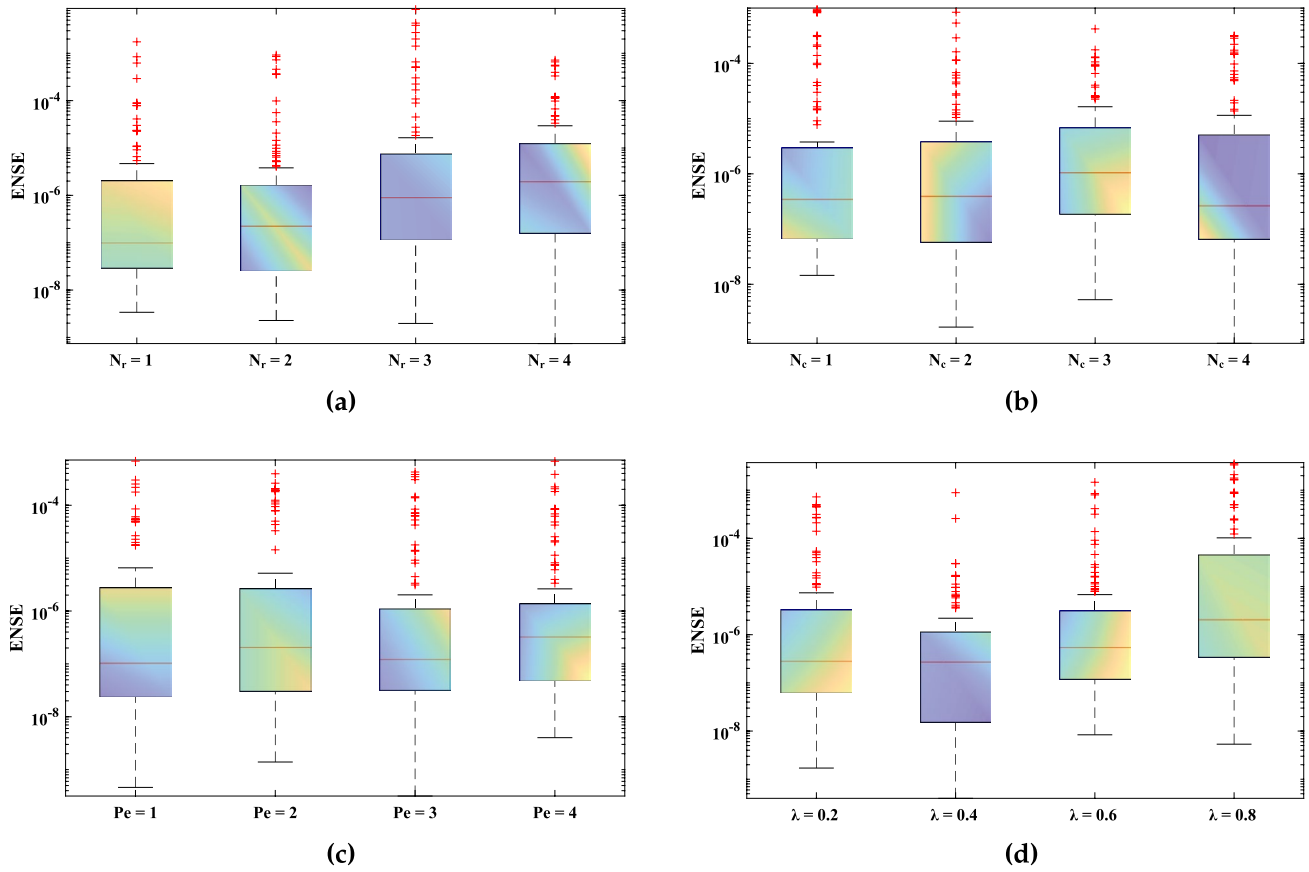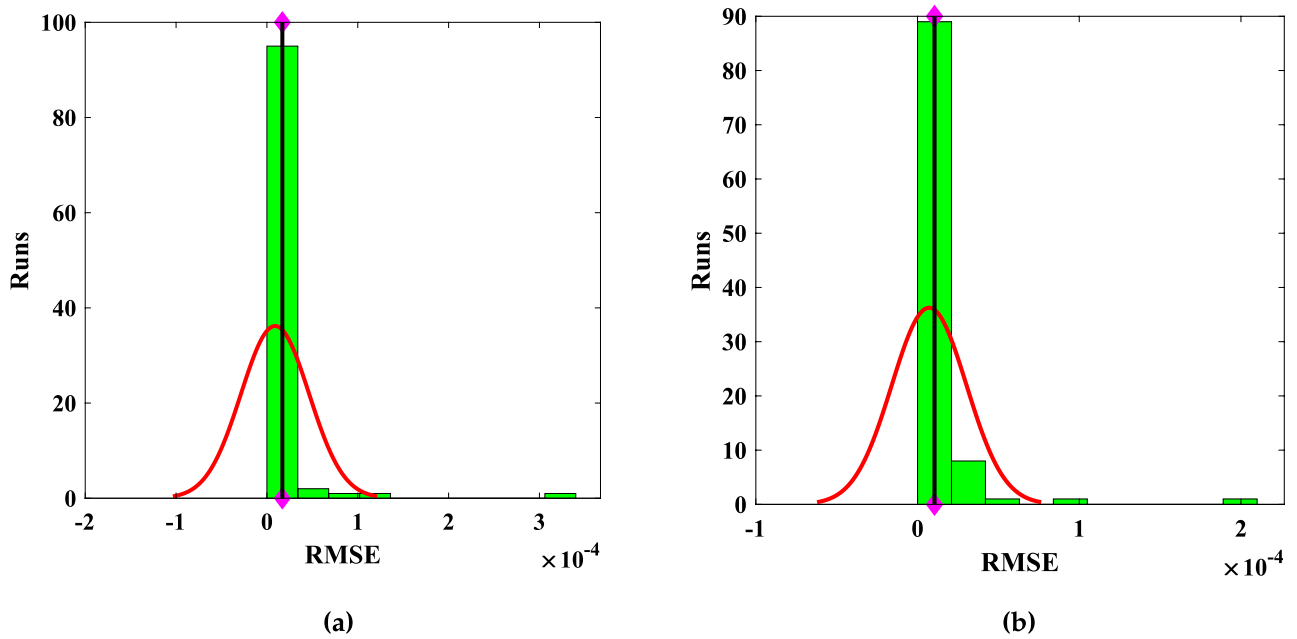**Fig. 13** Normal distribution curves for root mean square error in the solutions of the proposed technique for $Nr = 1 = Nr$ with $\lambda = 0.2, Pe = 2$ and $\gamma = 1$. Black line shows the minimum value

electrical impedance tomography, image inpainting, google mobility data to predict COVID-19 in Arizona, and prostate tumor growth under intermittent hormone therapy.

Appendix

Analytical expressions for the approximate solutions for $N_r = 1, 2, 3, 4$ with $\gamma = 1, \lambda = 0.4, Pe = 2, N_c = 2$.

$$\Theta(\eta) = \begin{cases} \dfrac{-5.21360882805874}{1+e^{-(-1.01053396078449\eta-0.44900736360641)}} + \dfrac{4.88533757656074}{1+e^{-(-1.44122641447643\eta-2.11729669435494)}} \\ + \dfrac{-0.20251640502463}{1+e^{-(-0.29736983240276\eta-1.42395337481997)}} + \dfrac{-3.57799973836620}{1+e^{(0.16509695901167\eta-1.66798630705047)}} \\ + \dfrac{9.48113483035763}{1+e^{-(-0.71254162909753\eta-1.00927081905381)}} + \dfrac{5.04658692622129}{1+e^{(2.21191327998701\eta-5.76209303631899)}} \\ + \dfrac{-1.01864981955383}{1+e^{-(-1.57975012332730\eta-2.25014200545541)}} + \dfrac{0.13530944582815}{1+e^{(-0.48318775124115\eta-0.33254256600736)}} \\ + \dfrac{0.87215189557398}{1+e^{-(-0.05748711596177\eta-0.82343035096074)}} + \dfrac{0.42201000537768}{1+e^{(2.45568769212668\eta+1.41614041290965)}} \end{cases}, \tag{A1}$$

$$\Theta(\eta) = \begin{cases} \dfrac{7.4933178007414}{1+e^{-(-2.80929691689061\eta-4.1653929366849)}} + \dfrac{0.2687689631323}{1+e^{-(-1.0670879776878\eta-0.1528474739736)}} \\ + \dfrac{0.2698744970625}{1+e^{-(-2.282231083141\eta-0.47315088034545)}} + \dfrac{4.5742774039661}{1+e^{(2.5188530249032\eta-6.2683014824533)}} \\ + \dfrac{-4.0953157574549}{1+e^{-(-0.641062298978\eta-2.02253514801403)}} + \dfrac{0.6844594153886}{1+e^{-(-0.5256097542600\eta-0.6973725199048)}} \\ + \dfrac{0.7481266765667}{1+e^{-(-0.4508471596743\eta-0.7593279861702)}} + \dfrac{0.6880731206857}{1+e^{(-0.5177704801665\eta-0.6761001982076)}} \\ + \dfrac{0.4329883005470}{1+e^{-(-0.7774796936049\eta-0.23197284230006)}} + \dfrac{0.7228436254854}{1+e^{-(-0.4753814269749\eta-0.7105482722214)}} \end{cases}, \tag{A2}$$

$$\Theta(\eta) = \begin{cases} \dfrac{0.4633591792998}{1+e^{-(0.7457126430757\eta+1.1802655985906)}} + \dfrac{1.2912356133131}{1+e^{-(-1.3434703034278\eta+0.0578086493869)}} \\ + \dfrac{-0.1416753085715}{1+e^{-(0.0382857260029\eta+0.8409830230890)}} + \dfrac{-1.7823560329379}{1+e^{-(-0.6738486241425\eta-2.6793887934288)}} \\ + \dfrac{0.3355768351387}{1+e^{-(-2.7178866894439\eta-0.4442774158027)}} + \dfrac{3.4246885090888}{1+e^{(-2.9152189666203\eta-6.7162336888586)}} \\ + \dfrac{-2.1442501692609}{1+e^{-(3.3564300714769\eta-10.8389170398741)}} + \dfrac{0.1163271790637}{1+e^{(0.0561738419760\eta+0.8910624877430)}} \\ + \dfrac{11.7088067626395}{1+e^{-(-2.9180380981997\eta-3.8367795150094)}} + \dfrac{-4.3123881745255}{1+e^{-(-1.8413918221509\eta-2.7054467279667)}} \end{cases}, \tag{A3}$$

$$\Theta(\eta) = \begin{cases} \dfrac{1.7448323822938}{1+e^{-(-2.2302302257691\eta-7.7760488944103)}} + \dfrac{-8.7967689605889}{1+e^{-(-1.0835003872559\eta-1.6756301853457)}} \\ + \dfrac{6.2614319596508}{1+e^{-(0.6137298409546\eta-3.3517594238915)}} + \dfrac{1.5099427798736}{1+e^{-(-0.7503844942517\eta+0.3367368597043)}} \\ + \dfrac{4.0710253118161}{1+e^{-(-2.9586496427078\eta-7.1506418220803)}} + \dfrac{7.7191955191471}{1+e^{(0.5495906929767\eta-3.6326563989930)}} \\ + \dfrac{8.7275041209682}{1+e^{-(-3.8059982466729\eta-4.1467016314529)}} + \dfrac{1.7324085426312}{1+e^{-(-0.7392821456043\eta+0.1621182391973)}} \\ + \dfrac{-1.7401223037523}{1+e^{-(-0.0031717813617\eta+1.5874367405918)}} + \dfrac{1.6520918427318}{1+e^{-(-1.0004145732286\eta+0.2158603652323)}} \end{cases}, \tag{A4}$$

Analytical expressions for the approximate solutions for $N_c = 1, 2, 3, 4$ with $\gamma = 1, \lambda = 0.4, Pe = 2, N_r = 2$.

$$\Theta(\eta) = \begin{cases} \dfrac{1.184502615791}{1+e^{-(-1.466458575649\eta+2.441374214687)}} + \dfrac{2.770010595143}{1+e^{-(-2.157231744333\eta-1.672663367064)}} \\ + \dfrac{2.854901956998}{1+e^{-(-2.142635357032\eta-1.632044873338)}} + \dfrac{-0.617379030047}{1+e^{-(-0.186608875911\eta+0.993250138736)}} \\ + \dfrac{8.646256622631}{1+e^{-(1.769093137951\eta-5.289680639832)}} + \dfrac{19.997481159157}{1+e^{-(-6.431939798760\eta-10.001381879743)}} \\ + \dfrac{2.328139077668}{1+e^{-(-2.192822451659\eta-1.824725661056)}} + \dfrac{-5.674560833584}{1+e^{-(-2.361551810308\eta-1.575364740336)}} \\ + \dfrac{-0.150953173260}{1+e^{-(-2.225494724337\eta-1.419520027503)}} + \dfrac{0.677736613078}{1+e^{-(-2.692772395122\eta-1.849011422743)}} \end{cases}, \tag{A5}$$

$$\Theta(\eta) = \begin{cases} \dfrac{0.250299133869}{1+e^{-(0.338978618770\eta+0.367165889627)}} + \dfrac{-0.007581459193}{1+e^{-(4.258779345303\eta+0.359596789883)}} \\ + \dfrac{0.644996496920}{1+e^{-(2.151594220482\eta+0.704059791422)}} + \dfrac{-1.757683021127}{1+e^{(-3.086110901370\eta+6.367148305277)}} \\ + \dfrac{0.458131587396}{1+e^{-(0.743184426254\eta+4.884402143126)}} + \dfrac{0.051770495543}{1+e^{-(4.328104803882\eta+1.421470720907)}} \\ + \dfrac{0.247248082475}{1+e^{-(0.334669723900\eta+0.368860616753)}} + \dfrac{118.431972124685}{1+e^{(-1.092323232010\eta-4.663747291436)}} \\ + \dfrac{0.041939897199}{1+e^{-(3.261678816010\eta+1.292740209004)}} + \dfrac{0.670442828780}{1+e^{(0.955508133661\eta+0.377351178863)}} \end{cases}, \tag{A6}$$

$$\Theta(\eta) = \begin{cases} \dfrac{0.971022275249}{1+e^{-(-0.052206943820\eta-0.697786381092)}} + \dfrac{0.979461623426}{1+e^{-(-0.058869715723\eta-0.711442262079)}} \\ + \dfrac{0.320885257819}{1+e^{-(-0.681177802285\eta+4.257007464462)}} + \dfrac{-3.594817757691}{1+e^{-(-2.766766341473\eta+6.315744316553)}} \\ + \dfrac{1.015324288405}{1+e^{-(-0.082110578184\eta-0.764673615706)}} + \dfrac{-1.586633563021}{1+e^{-(-1.684851608347\eta+1.312028419628)}} \\ + \dfrac{33.777432407549}{1+e^{-(-3.459111505289\eta-6.429966603374)}} + \dfrac{0.986160316039}{1+e^{(0.176795327\eta-2.006129937)}} \\ + \dfrac{-2.092392395}{1+e^{-(-0.062119767978\eta-0.719166855051)}} + \dfrac{0.961353543912}{1+e^{-(-0.056741135628\eta-0.699650675619)}} \end{cases}, \tag{A7}$$

$$\Theta(\eta) = \begin{cases} \dfrac{-0.197737939083}{1+e^{-(-4.726961545859\eta-1.027983701793)}} + \dfrac{4.695407576385}{1+e^{-(2.378780180150\eta-4.829315877708)}} \\ + \dfrac{0.324457968422}{1+e^{-(-0.220686279862\eta-0.102010316759)}} + \dfrac{0.364302660136}{1+e^{-(-0.249692951293\eta-0.103988496229)}} \\ + \dfrac{0.155096405820}{1+e^{-(-0.092251707502\eta-0.090969121068)}} + \dfrac{3.807064634057}{1+e^{-(-2.149021552692\eta-1.623509551746)}} \\ + \dfrac{-1.997328911723}{1+e^{-(2.314866467748\eta-3.981652365937)}} + \dfrac{0.144807091085}{1+e^{-(-0.084134974309\eta-0.083146712892)}} \\ + \dfrac{-0.212346045507}{1+e^{-(-3.361094334884\eta+0.175515512032)}} + \dfrac{0.145456615657}{1+e^{-(-0.082233516473\eta-0.082228986034)}} \end{cases}, \tag{A8}$$

Analytical expressions for the approximate solutions of $Pe = 1, 2, 3, 4$ with $\gamma = 1, \lambda = 0.4, N_r = N_c = 2$.

$$\Theta(\eta) = \begin{cases} \dfrac{0.698651621195}{1+e^{-(-0.092973087832\eta-0.382354864417)}} + \dfrac{5.003299292728}{1+e^{-(-0.102662327983\eta+0.326844808829)}} \\ + \dfrac{0.698807418169}{1+e^{-(-0.093656545201\eta-0.378926690890)}} + \dfrac{0.700437233718}{1+e^{-(-0.093005650214\eta-0.378260795299)}} \\ + \dfrac{0.696899715218}{1+e^{-(-0.095109141923\eta-0.377305115081)}} + \dfrac{-3.912967156172}{1+e^{-(-1.789601393569\eta+4.820052759095)}} \\ + \dfrac{0.701218209499}{1+e^{-(-0.095079756913\eta+-0.374881493324)}} + \dfrac{-0.739582680758}{1+e^{-(-2.523060932663x-1.793445449061)}} \\ + \dfrac{5.405527126151}{1+e^{-(-1.896665396755\eta-2.600250169199)}} + \dfrac{0.700968681351}{1+e^{-(-0.094828563665\eta-0.375635835030)}} \end{cases}, \tag{A9}$$

$$\Theta(\eta) = \begin{cases} \dfrac{-0.146895111171}{1+e^{-(1.684562794695\eta+1.376449571964)}} + \dfrac{8.542219217026}{1+e^{-(-2.453371811068\eta-5.084980594422)}} \\ + \dfrac{1.580699641940}{1+e^{-(-0.096392168193\eta-1.046842651743)}} + \dfrac{1.323270009238}{1+e^{-(-0.789808717574\eta-1.236307150920)}} \\ + \dfrac{0.988985201114}{1+e^{-(-1.010618457480\eta-1.356678862921)}} + \dfrac{2.089458955960}{1+e^{(2.715589984086\eta-5.919835339317)}} \\ + \dfrac{-3.062374668264}{1+e^{-(-0.206367895962x-0.636523956579)}} + \dfrac{1.529210448939}{1+e^{-(-0.228659397006\eta-1.088410256422)}} \\ + \dfrac{1.581012476393}{1+e^{-(-0.096628103746\eta-1.046289538362)}} + \dfrac{1.584537376584}{1+e^{-(-0.081453226658\eta-1.047393712082)}} \end{cases}, \tag{A10}$$

$$\Theta(\eta) = \begin{cases} \dfrac{1.361977041068}{1+e^{-(-1.055557851038\eta-0.942772526058)}} + \dfrac{-0.506512451450}{1+e^{-(-0.137134690491\eta-1.414754744984)}} \\ + \dfrac{0.931094493851}{1+e^{-(-0.001538266473\eta+3.932550422437)}} + \dfrac{0.608664339299}{1+e^{-(-0.071963903117\eta+1.780548823824)}} \\ + \dfrac{0.344788290676}{1+e^{-(-0.071019311724\eta-0.000172613392)}} + \dfrac{0.895073208073}{1+e^{-(-0.081611115919\eta+0.061423432621)}} \\ + \dfrac{3.350607037659}{1+e^{-(-2.337678425422\eta-4.129454086851)}} + \dfrac{0.040406163850}{1+e^{-(-0.131422996505x-0.034847399700)}} \\ + \dfrac{-1.596628176332}{1+e^{-(-3.444037272108\eta+6.730829771338)}} + \dfrac{0.342381149808}{1+e^{-(-0.073943007277\eta+0.001000557191)}} \end{cases}, \tag{A11}$$

$$\Theta(\eta) = \begin{cases} \dfrac{-2.030493960849}{1+e^{-(2.306176211650\eta-4.738655341951)}} + \dfrac{2.218753085277}{1+e^{(-0.148532911492\eta+0.014962879384)}} \\ + \dfrac{-0.710316300405}{1+e^{-(0.510027151502\eta-1.170498640292)}} + \dfrac{0.818217958502}{1+e^{-(1.414919281337\eta-0.116961531347)}} \\ + \dfrac{-0.089599630495}{1+e^{(-1.307614600452\eta-1.006543681877)}} + \dfrac{5.830521990353}{1+e^{-(2.990137016752\eta-6.553594887424)}} \\ + \dfrac{-0.764844182196}{1+e^{-(0.757571462223\eta-1.013758439283)}} + \dfrac{1.143624227980}{1+e^{-(2.628732258973\eta-2.953285737685)}} \\ + \dfrac{-0.659099319769}{1+e^{-(0.298910992673\eta-0.643923031320)}} + \dfrac{0.238914811929}{1+e^{-(1.844273587106\eta-0.831090515001)}} \end{cases},$$

(A12)

Analytical expressions for the approximate solutions of $\lambda = 0.2, 0.4, 0.6, 0.8$ with $Pe = 2, \gamma = 1, N_r = N_c = 2$.

$$\Theta(\eta) = \begin{cases} \dfrac{-3.781383325749}{1+e^{-(2.347290376790\eta+5.383949756846)}} + \dfrac{1.912173140048}{1+e^{-(0.583630397668\eta+0.024850942327)}} \\ + \dfrac{-1.558705585584}{1+e^{-(1.912946787560\eta-2.646487482227)}} + \dfrac{1.766415918623}{1+e^{-(0.058173416653\eta-1.166779973996)}} \\ + \dfrac{1.550609866723}{1+e^{(0.128182557220x-0.985102247883)}} + \dfrac{5.691161109220}{1+e^{-(0.342633523414\eta-0.407424968978)}} \\ + \dfrac{-1.538122866466}{1+e^{-(2.404212320455\eta-2.107965202164)}} + \dfrac{32.958478543652}{1+e^{-(1.802112580628\eta-3.972260831035)}} \\ + \dfrac{1.542667449233}{1+e^{(0.937061313882\eta-3.559710057918)}} + \dfrac{-2.900316627244}{1+e^{(0.133571942108\eta-0.975914348535)}} \end{cases},$$

(A13)

$$\Theta(\eta) = \begin{cases} \dfrac{-1.111076945924}{1+e^{-(1.219749571488\eta-0.221330398503)}} + \dfrac{-1.201927299972}{1+e^{-(0.967208794649\eta-0.904717750898)}} \\ + \dfrac{13.645185283690}{1+e^{-(2.948087635852\eta-5.054746487468)}} + \dfrac{1.143789269027}{1+e^{(0.296687742611\eta-0.326336879992)}} \\ + \dfrac{0.943932248193}{1+e^{-(1.743896145916\eta-0.734847901139)}} + \dfrac{1.294998242580}{1+e^{-(0.633667318097)\eta}} \\ + \dfrac{0.159638946195}{1+e^{(1.561969466343\eta+1.571780193139)}} + \dfrac{-2.076385341372}{1+e^{-(0.311928231850\eta-3.797867169826)}} \\ + \dfrac{0.630202579653}{1+e^{-(0.370673088136\eta+0.734673440429)}} + \dfrac{3.395839494015}{1+e^{-(2.616401814548\eta-6.154809519902)}} \end{cases},$$

(A14)

$$\Theta(\eta) = \begin{cases} \dfrac{0.739610430026}{1+e^{-(1.604896776388\eta-0.739559941731)}} + \dfrac{0.393314479289}{1+e^{(0.145045979505\eta-0.194907129034)}} \\ + \dfrac{-1.650413371969}{1+e^{(0.310080869587\eta-1.984570924656)}} + \dfrac{0.196124137971}{1+e^{(0.276333660732\eta-0.141438884880)}} \\ + \dfrac{0.141168236757}{1+e^{(0.326702774792\eta-0.155157215080)}} + \dfrac{-1.952031926853}{1+e^{-(1.628877830988\eta-4.941519544420)}} \\ + \dfrac{0.206954577700}{1+e^{(0.276301097483\eta-0.159151839371)}} + \dfrac{77.829990745035}{1+e^{-(2.634872738873\eta-6.628381131366)}} \\ + \dfrac{5.436193560530}{1+e^{(2.716751742751\eta-6.844575036172)}} + \dfrac{1.059044460482}{1+e^{-(0.023579591639\eta-0.354410865023)}} \end{cases},$$

(A15)

$$\Theta(\eta) = \begin{cases} \dfrac{0.293243581386}{1+e^{-(1.922816247792\eta-0.141514802019)}} + \dfrac{0.220070557690}{1+e^{-(0.023451791134\eta+0.013431411599)}} \\ + \dfrac{-3.371963852712}{1+e^{(1.198910649668\eta-7.077946204310)}} + \dfrac{0.322051785039}{1+e^{-(0.376938234033\eta+0.045276581898)}} \\ + \dfrac{0.180677627453}{1+e^{(0.240346794270\eta+0.074908745480)}} + \dfrac{0.278377329709}{1+e^{-(0.238009071233\eta+0.029535987840)}} \\ + \dfrac{8.091210083932}{1+e^{-(2.404742277837\eta-4.267535154433)}} + \dfrac{0.247874459227}{1+e^{(1.621813111073\eta+0.044924173335)}} \\ + \dfrac{0.232414371342}{1+e^{-(0.055515398530\eta+0.009064800456)}} + \dfrac{6.264609304470}{1+e^{-(3.294591488970\eta-8.861691812633)}} \end{cases},$$

(A16)

Author Contributions All authors contributed equally to finalize and approve the final version of the manuscript.

Declarations

Conflict of interest All of the authors of this publication have confirmed that they do not have any competing interests with relation to this manuscript.

Replication of results The corresponding author will provide access to the data used in this work upon reasonable request.

References

Abualigah L, Diabat A, Mirjalili S, Abd Elaziz M, Gandomi AH (2021) The arithmetic optimization algorithm. Comput Methods Appl Mech Eng 376:113609

Alarie S, Audet C, Gheribi AE, Kokkolaras M, Le Digabel S (2021) Two decades of blackbox optimization applications. EURO J Comput Optim 9:100011

Alkam MK, Al-Nimr MA (1999) Solar collectors with tubes partially filled with porous substrates. ASME J Sol Energy Eng 121(1):20–24

Audet C (2014) A survey on direct search methods for blackbox optimization and their applications. Mathematics without boundaries. Springer, New York, pp 31–56

Audet C, Hare W (2017) Derivative-free and blackbox optimization, vol 2. Springer, Berlin

Audet C, Le Digabel S, Saltet R (2022a) Quantifying uncertainty with ensembles of surrogates for blackbox optimization. Comput Optim Appl 83:29–66

Audet C, Digabel SL, Salomon L, Tribes C (2022b) Constrained blackbox optimization with the NOMAD solver on the COCO constrained test suite. In: Proceedings of the genetic and evolutionary computation conference companion, pp 1683–1690

Aydoğdu İ, Saka MP (2012) Ant colony optimization of irregular steel frames including elemental warping effect. Adv Eng Softw 44:150–169

Aydoğdu İ, Akın A, Saka MP (2016) Design optimization of real world steel space frames using artificial bee colony algorithm with Levy flight distribution. Adv Eng Softw 92:1–14

Aziz A, Makinde O (2010) Heat transfer and entropy generation in a two-dimensional orthotropic convection pin fin. Int J Exergy 7:579–592

Baslem A, Sowmya G, Gireesha B, Prasannakumara B, Rahimi-Gorji M, Hoang NM (2020) Analysis of thermal behavior of a porous fin fully wetted with nanofluids: convection and radiation. J Mol Liq 307:112920

Ben-Nakhi A, Chamkha AJ (2006) Effect of length and inclination of a thin fin on natural convection in a square enclosure. Numer Heat Transf 50:381–399

Buonomo B, Cascetta F, Manca O, Sheremet M (2021) Heat transfer analysis of rectangular porous fins in local thermal non-equilibrium model. Appl Therm Eng 195:117237

Chamkha AJ, Mansour M, Ahmed SE (2010) Double-diffusive natural convection in inclined finned triangular porous enclosures in the presence of heat generation/absorption effects. Heat Mass Transf 46:757–768

Cuce E, Cuce PM (2015) A successful application of homotopy perturbation method for efficiency and effectiveness assessment of longitudinal porous fins. Energy Convers Manage 93:92–99

Cui Y, Hong Y, Khan NA, Sulaiman M (2021) Application of soft computing paradigm to large deformation analysis of cantilever beam under point load. Complexity. https://doi.org/10.1155/2021/2182693

Dalla CER, da Silva WB, Dutra JCS, Colaço MJ (2021) A comparative study of gradient-based and meta heuristic optimization methods using Griewank benchmark function. Braz J Dev 7:55341–55350

Das R, Kundu B (2020) Estimating magnetic field strength in a porous fin from a surface temperature response. Electron Lett 56:1011–1013

Deshamukhya T, Bhanja D, Nath S, Hazarika SA (2018) Prediction of optimum design variables for maximum heat transfer through a rectangular porous fin using particle swarm optimization. J Mech Sci Technol 32:4495–4502

Dhiman G, Kaur A (2019) STOA: a bio-inspired based optimization algorithm for industrial engineering problems. Eng Appl Artif Intell 82:148–174

Dinarvand S, Hosseini R (2013) Optimal homotopy asymptotic method for convective-radiative cooling of a lumped system, and convective straight fin with temperature-dependent thermal conductivity. Afr Matematika 24:103–116

Domairry G, Fazeli M (2009) Homotopy analysis method to determine the fin efficiency of convective straight fins with temperature-dependent thermal conductivity. Commun Nonlinear Sci Numer Simul 14:489–499

Erdal F, Doğan E, Saka MP (2011) Optimum design of cellular beams using harmony search and particle swarm optimizers. J Constr Steel Res 67:237–247

Fallah Najafabadi M, Talebi Rostami H, Hosseinzadeh K, Domiri Ganji D (2021) Thermal analysis of a moving fin using the radial basis function approximation. Heat Transf 50:7553–7567

Fox V, Erickson L, Fan L (1969) The laminar boundary layer on a moving continuous flat sheet immersed in a non-Newtonian fluid. AIChE J 15:327–333

Gireesha B, Sowmya G (2020) Heat transfer analysis of an inclined porous fin using differential transform method. Int J Ambient Energy 43:3189–3195

Gul RN, Ahmad A, Fayyaz S, Sattar MK, Saddam ul Haq S (2021) A hybrid flower pollination algorithm with sequential quadratic programming technique for solving dynamic combined economic emission dispatch problem. Mehran Univ Res J Eng Technol 40:371–382

He J, Peng Z, Cui D, Qiu J, Li Q, Zhang H (2022) Enhanced sooty tern optimization algorithm using multiple search guidance strategies and multiple position update modes for solving optimization problems. Appl Intell https://doi.org/10.1007/s10489-022-03635-9

Hoshyar H, Ganji D, Abbasi M (2015) Analytical solution for Porous Fin with temperature-dependent heat generation via Homotopy perturbation method. Int J Adv Appl Math Mech 2:15–22

Hosseinzadeh S, Hosseinzadeh K, Hasibi A, Ganji D (2022) Thermal analysis of moving porous fin wetted by hybrid nanofluid with trapezoidal, concave parabolic and convex cross sections. Case Stud Therm Eng 30:101757

Hsiang NJ, Selvarajoo A, Arumugasamy SK (2020) Artificial neural network modelling for slow pyrolysis process of biochar from banana peels and its effect on O/C ratio. In: International conference on innovative technology, engineering and science, Springer, pp 336–350

Huang W, Jiang T, Zhang X, Khan NA, Sulaiman M (2021) Analysis of beam-column designs by varying axial load with internal forces and bending rigidity using a new soft computing technique. Complexity. https://doi.org/10.1155/2021/6639032

Hung HM, Appl FC (1967) Heat transfer of thin fins with temperature-dependent thermal properties and internal heat generation. ASME J Heat Transfer 89(2):155–162

Khan NA, Alshammari FS, Romero CAT, Sulaiman M, Laouini G (2021a) Mathematical analysis of reaction-diffusion equations modeling the Michaelis-Menten kinetics in a micro-disk biosensor. Molecules 26:7310

Khan NA, Alshammari FS, Romero CAT, Sulaiman M, Mirjalili S (2021b) An optimistic solver for the mathematical model of the flow of Johnson Segalman fluid on the surface of an infinitely long vertical cylinder. Materials 14:7798

Khan NA, Khalaf OI, Romero CAT, Sulaiman M, Bakar MA (2021c) Application of Euler neural networks with soft computing paradigm to solve nonlinear problems arising in heat transfer. Entropy 23:1053

Khan NA, Sulaiman M, Kumam P, Bakar MA (2021d) Thermal analysis of conductive-convective-radiative heat exchangers with temperature dependent thermal conductivity. IEEE Access 9:138876–138902

Khan NA, Sulaiman M, Tavera Romero CA, Alarfaj FK (2021e) Theoretical analysis on absorption of carbon dioxide (CO_2) into solutions of phenyl glycidyl ether (PGE) using nonlinear autoregressive exogenous neural networks. Molecules 26:6041

Khan NA, Sulaiman M, Kumam P, Alarfaj FK (2022a) Application of Legendre polynomials based neural networks for the analysis of heat and mass transfer of a non-Newtonian fluid in a porous channel. Adv Contin Discrete Models 2022:1–32

Khan NA, Sulaiman M, Tavera Romero CA, Alshammari FS (2022b) Analysis of nanofluid particles in a duct with thermal radiation by using an efficient metaheuristic-driven approach. Nanomaterials 12:637

Kiwan S (2007) Effect of radiative losses on the heat transfer from porous fins. Int J Therm Sci 46:1046–1055

Kiwan S, Al-Nimr M (2001) Using porous fins for heat transfer enhancement. J Heat Transf 123:790–795

Kiwan S, Zeitoun O (2008) Natural convection in a horizontal cylindrical annulus using porous fins. Int J Numer Methods Heat Fluid Flow. https://doi.org/10.1108/09615530810879747

Kiwan S, Alwan H, Abdelal N (2020) An experimental investigation of the natural convection heat transfer from a vertical cylinder using porous fins. Appl Therm Eng 179:115673

Kumar S, Jangir P, Tejani GG, Premkumar M, Alhelou HH (2021a) MOPGO: a new physics-based multi-objective plasma generation optimizer for solving structural optimization problems. IEEE Access 9:84982–85016

Kumar S, Tejani GG, Pholdee N, Bureerat S (2021b) Multiobjecitve structural optimization using improved heat transfer search. Knowl-Based Syst 219:106811

Kumar S, Tejani GG, Pholdee N, Bureerat S (2021c) Multi-objective passing vehicle search algorithm for structure optimization. Expert Syst Appl 169:114511

Kundu B, Yook SJ (2021) An accurate approach for thermal analysis of porous longitudinal, spine and radial fins with all nonlinearity effects-analytical and unified assessment. Appl Math Comput 402:126124

Ma J, Sun Y, Li B (2017) Spectral collocation method for transient thermal analysis of coupled conductive, convective and radiative heat transfer in the moving plate with temperature dependent properties and heat generation. Int J Heat Mass Transf 114:469–482

Moitsheki R, Rashidi M, Basiriparsa A, Mortezaei A (2015) Analytical solution and numerical simulation for one-dimensional steady nonlinear heat conduction in a longitudinal radial fin with various profiles. Heat Transf-Asian Res 44:20–38

Ndlovu P, Moitsheki R (2018) Thermal analysis of natural convection and radiation heat transfer in moving porous fins. Front Heat Mass Transf (FHMT). https://doi.org/10.5098/hmt.12.7

Nguyen QH, Ly HB, Nguyen TA, Phan VH, Nguyen LK, Tran VQ (2021) Investigation of ANN architecture for predicting shear strength of fiber reinforcement bars concrete beams. PLoS ONE 16:e0247391

Patel T, Meher R (2015) A study on temperature distribution, efficiency and effectiveness of longitudinal porous fins by using adomian decomposition sumudu transform method. Procedia Eng 127:751–758

Rashid MFFA (2021) Tiki-taka algorithm: a novel metaheuristic inspired by football playing style. Eng Comput 38(1):313–343

Razelos P, Kakatsios X (2000) Optimum dimensions of convecting-radiating fins: part I-longitudinal fins. Appl Therm Eng 20:1161–1192

Saka MP, Hasançebi O, Geem ZW (2016) Metaheuristics in structural optimization and discussions on harmony search algorithm. Swarm Evolut Comput 28:88–97

Sarwe DU, Kulkarni VS (2021) Thermal behaviour of annular hyperbolic fin with temperature dependent thermal conductivity by differential transformation method and Pade approximant. Phys Scr 96:105213

Selimefendigil F, Öztop HF (2012) Fuzzy-based estimation of mixed convection heat transfer in a square cavity in the presence of an adiabatic inclined fin. Int Commun Heat Mass Transf 39:1639–1646

Şenol M, Timuçin Dolapçı İ, Aksoy Y, Pakdemirli M (2013) Perturbation-iteration method for first-order differential equations and systems. In: Abstract and applied analysis, vol 2013. Hindawi, London

Sheikholeslami M, Ganji DD (2018) Applications of semi-analytical methods for nanofluid flow and heat transfer. Elsevier, Amsterdam

Singh P, Kottath R, Tejani GG (2022) Ameliorated follow the leader: algorithm and application to truss design problem. Structures 42:181–204

Sobamowo M, Oguntala G, Yinusa A, Adedibu A (2019) Analysis of transient heat transfer in a longitudinal fin with functionally graded material in the presence of magnetic field using finite difference method. World Sci News 137:166–187

Sowmya G, Gireesha B, Makinde O (2019) Thermal performance of fully wet longitudinal porous fin with temperature-dependent thermal conductivity, surface emissivity and heat transfer coefficient. Multidisc Model Mater Struct. https://doi.org/10.1108/mmms-08-2019-0147

Starostenko O, Ramírez A, Zehe A, Burlak G (2005) Novel algorithms for estimating motion characteristics within a limited sequence of images. Recent advances in multidisciplinary applied physics. Elsevier, Amsterdam, pp 277–281

Sun SW, Li XF (2020) Exact solution of the nonlinear fin problem with exponentially temperature-dependent thermal conductivity and heat transfer coefficient. Pramana 94:1–10

Tahani M, Vakili M, Khosrojerdi S (2016) Experimental evaluation and ANN modeling of thermal conductivity of graphene oxide nanoplatelets/deionized water nanofluid. Int Commun Heat Mass Transf 76:358–365

Taklifi A, Aghanajafi C, Akrami H (2010) The effect of MHD on a porous fin attached to a vertical isothermal surface. Transp Porous Media 85:215–231

Talgorn B, Kokkolaras M, DeBlois A, Piperni P (2017) Numerical investigation of non-hierarchical coordination for distributed multidisciplinary design optimization with fixed computational budget. Struct Multidisc Optim 55:205–220

Tejani G, Savsani V, Patel V (2017) Modified sub-population based heat transfer search algorithm for structural optimization. Int J Appl Metaheuristic Comput (IJAMC) 8:1–23

Tejani GG, Savsani VJ, Patel VK, Savsani PV (2018) Size, shape, and topology optimization of planar and space trusses using mutation-based improved metaheuristics. J Comput Des Eng 5:198–214

Tejani GG, Pholdee N, Bureerat S, Prayogo D, Gandomi AH (2019a) Structural optimization using multi-objective modified adaptive symbiotic organisms search. Expert Syst Appl 125:425–441

Tejani GG, Savsani VJ, Patel VK, Mirjalili S (2019b) An improved heat transfer search algorithm for unconstrained optimization problems. J Comput Des Eng 6:13–32

Tejani GG, Kumar S, Gandomi AH (2021) Multi-objective heat transfer search algorithm for truss optimization. Eng Comput 37:641–662

Tian H, Wang K, Yu B, Song C, Jermsittiparsert K (2021) Hybrid improved Sparrow Search Algorithm and sequential quadratic programming for solving the cost minimization of a hybrid photovoltaic, diesel generator, and battery energy storage system. Energy Sources A. https://doi.org/10.1080/15567036.2021.1905111

Turkyilmazoglu M (2018) Heat transfer from moving exponential fins exposed to heat generation. Int J Heat Mass Transf 116:346–351

Umar M, Raja MAZ, Sabir Z, Alwabli AS, Shoaib M (2020) A stochastic computational intelligent solver for numerical treatment of mosquito dispersal model in a heterogeneous environment. Eur Phys J Plus 135:1–23

Massan SUR, Wagan AI, Shaikh MM (2020) A new metaheuristic optimization algorithm inspired by human dynasties with an application to the wind turbine micrositing problem. Appl Soft Comput 90:106176

Wang J, Hu H, Zhang W, Hu Z (2021) Optimization-based transient control of turbofan engines: a sequential quadratic programming approach. Int J Turbo Jet-Engines. https://doi.org/10.1515/tjj-2021-0072

Welhazi Y, Guesmi T, Alshammari BM, Alqunun K, Alateeq A, Almalaq Y, Alsabhan R, Abdallah HH (2022) A novel hybrid chaotic Jaya and sequential quadratic programming method for robust design of power system stabilizers and static VAR compensator. Energies 15:860

Yang C, Wang M, Wang W, Pu Z, Ma M (2021) An efficient vehicle-following predictive energy management strategy for PHEV based on improved sequential quadratic programming algorithm. Energy 219:119595

Ye WB (2017) Enhanced latent heat thermal energy storage in the double tubes using fins. J Therm Anal Calorim 128:533–540

Yousif S, Saka M (2021) Enhanced beetle antenna search: a swarm intelligence algorithm. Asian J Civil Eng 22:1185–1219

Zaeimi M, Ghoddosian A (2020) Color harmony algorithm: an art-inspired metaheuristic for mathematical function optimization. Soft Comput 24:12027–12066

Zhao TH, Khan MI, Chu YM (2021) Artificial neural networking (ANN) analysis for heat and entropy generation in flow of non-Newtonian fluid between two rotating disks. Math Methods Appl Sci. https://doi.org/10.1002/mma.7310

Zhao W, Wang L, Mirjalili S (2022) Artificial hummingbird algorithm: a new bio-inspired optimizer with its engineering applications. Comput Methods Appl Mech Eng 388:114194

Zhu G, Wen T, Zhang D (2021) Machine learning based approach for the prediction of flow boiling/condensation heat transfer performance in mini channels with serrated fins. Int J Heat Mass Transf 166:120783

Authors and Affiliations

Naveed Ahmad Khan[1] · **Muhammad Sulaiman[1]** · **Fahad Sameer Alshammari[2]**

Fahad Sameer Alshammari
f.alshammari@psau.edu.sa

[1]   Department of Mathematics, Abdul Wali Khan University,
Mardan 23200, Pakistan

[2]   Department of Mathematics, College of Science
and Humanities in Alkharj, Prince Sattam bin Abdulaziz
University, Al-Kharj 11942, Saudi Arabia